ISSN 0972-0405

ISET JOURNAL OF EARTHQUAKE TECHNOLOGY

Vol. 46 | No. 1 | March 2009

CONTENTS

Financial Assistance from AICTE and DST, New Delhi for the Publication of ISET Journals for 2008–2009 is duly acknowledged.

ISET Journal of Earthquake Technology, Paper No. 500, Vol. 46, No. 1, March 2009, pp. 1–17

SMOOTH SPECTRA OF HORIZONTAL AND VERTICAL GROUND MOTIONS FOR IRAN

H. Ghasemi*, M. Zare** and F. Sinaeian***

*Seismology Research Center, International Institute of Earthquake Engineering and Seismology, Tehran, Iran
**Earthquake Research Institute, University of Tokyo, Tokyo, Japan
***Iran Strong Motion Network, Building and Housing Research Center, Tehran, Iran

ABSTRACT

In this study, several practical limitations of the current building code of Iran are addressed with respect to seismic hazard analysis (SHA) projects. The main concern of the present study is to propose a practical procedure for constructing smooth response spectra from the peak values of ground motion. The dynamic amplification factors are calculated for horizontal and vertical components, considering a selection of Iran's strong-motion records, and are compared with those proposed in the previous studies. The results and conclusions of this study are effective in the evaluation of the Iranian code and can be used in the SHA projects in Iran.

KEYWORDS: Smooth Response Spectra, Seismic Hazard Analysis, Iran

INTRODUCTION

Iranian plateau has long been known as an active seismic area in the world, which from time to time has suffered from destructive and catastrophic earthquakes, causing heavy loss of human lives and widespread damage. Recently, after the destructive earthquakes of Avaj in the year 2002, Bam earthquake of 2003, etc., there has been a considerable increase in the demand for performing site-specific seismic hazard analysis (SHA). While SHA provides the occurrence rate of future earthquake ground motions, the evaluation of the effects of these ground motions on the structural response is also strongly needed. The response of a structure to an earthquake motion can be evaluated using response spectra, which are defined as the graphic relationship between the maximum responses of single-degree-of-freedom (SDOF) systems and their natural periods. However, the individual response spectra of strong-motion records have jagged shapes with significant peaks and valleys and differ remarkably; hence, they can only be used to evaluate the seismic forces during specific earthquakes at certain sites (Newmark and Hall, 1969). As opposed to the response spectra, design response spectra, as suggested by several building codes, are extremely effective in identifying the loads during the probable earthquake ground motions in future.

Recent studies (e.g., Tehranizadeh and Hamedi, 2003; Ghodrati Amiri et al., 2003) on design response spectra in Iran are limited to the influence of ground motion parameters of Iran earthquakes and local site conditions on the design spectra. In the previous studies in Iran, the response spectra were normalized to peak ground accelerations (PGAs); however, as shown in several studies (Malhotra, 2006; Newmark and Hall, 1969; Hall et al., 1976), such normalization schemes are not proper for all frequency ranges. Furthermore, in the previous studies in Iran only horizontal (and not the vertical) components of ground motions were considered. In this study, the modified methodology proposed by Malhotra (2006) is followed in order to construct smooth response spectra for both horizontal and vertical components. Furthermore, smooth spectra are adjusted for different damping values. The data, recorded in Iran, is also used to establish relationships between the peak ground motion parameters, PGA, PGV, and PGD. In the current SHA projects in Iran, the most ordinary output parameter is PGA; however, to construct the smooth spectra, based on the methodology proposed by Malhotra (2006) and those described in several other studies (Newmark and Hall, 1969; Mohraz, 1976), it is indicated that peak ground motion parameters (PGA, PGV, and PGD) should be determined and due to weak correlation between these parameters, it is necessary that they be estimated independently.

The main motivation of this study is presented after a brief introduction to Iranian Code of Practice for Seismic Resistant Design, Standard No. 2800 (BHRC, 2003). The main characteristics of the selected strong-motion data bank are described thereafter. Then, the methodology as followed is described, and the results are presented. Subsequently, the results are compared with those of the similar studies, and the concluding remarks are given. Finally, a practical example on constructing smooth response spectrum, by using the proposed methodology, is presented.

LIMITATIONS OF STANDARD NO. 2800

Iran has had an earthquake code since the destructive earthquake of Boeen Zahra in the year 1962. Iranian code of practice for the seismic-resistant design of buildings (i.e., the so-called Standard No. 2800) (BHRC, 2003) was revised by the Building and Housing Research Center (BHRC) in 1987. It became mandatory after the Roodbar-Manjil earthquake in the year 1990. It has been revealed that most of the severely damaged and/or collapsed constructions due to the moderate-to-large earthquake ground motions were the ones, which had not followed the code (Zare, 2004).

In Standard No. 2800 (BHRC, 2003), the building factor (i.e., the normalized spectral acceleration) is calculated as follows:

$$B = \begin{cases} 1+S\left(\dfrac{T}{T_0}\right) & ;\ 0 \le T \le T_0 \\ 1+S & ;\ T_0 \le T \le T_S \\ (1+S)\left(\dfrac{T_S}{T}\right)^{2/3} & ;\ T \ge T_S \end{cases} \tag{1}$$

where T is the natural period of the building, T_0 and T_S are the control periods having fixed site-dependent values, as listed in Table 1; and S is the parameter that depends on the site class and hazard level. The corresponding S values for each category are listed in Table 1. The design response spectrum of the horizontal ground motion is obtained for each site by multiplying the building factor by PGA, which is based on the probabilistic seismic hazard analysis.

Table 1: Values for the T_0, T_S and S Factors Recommended in Standard No. 2800 for Different Site Categories

Site Class	T_0	T_S	S	
			Low-Moderate Hazard Level	High-Very High Hazard Level
I	0.10	0.4	1.50	1.50
II	0.10	0.5	1.50	1.50
III	0.15	0.7	1.75	1.75
IV	0.15	1.0	2.25	1.75

As mentioned above, PGA is recommended in Standard No. 2800 to derive design values for the entire period range. However, in some building codes the design response spectrum consists of two or three regions, for example, short, long, and very-long period ranges (e.g., ICC, 2003, 2006). In these codes, the design response spectrum is characterized in terms of spectral acceleration (SA) at specific periods, e.g., 0.2 and 1 s in ICC (2003). Actually, it is outlined in previous studies (e.g., Mohraz et al., 1973; Newmark and Hall, 1969) that the response spectra for earthquake ground motions can be divided into three general regions, namely, acceleration-sensitive, velocity-sensitive, and displacement-sensitive. It is assumed that SAs in each region are reasonably well-correlated to the corresponding peak ground motion parameters; hence, to construct each region, corresponding peak ground motion parameter, i.e., PGA, PGV, or PGD, should be used. This method of constructing response spectrum is better than the one, which uses spectral accelerations at the specified periods (say, 0.2 and 1 s), because PGA, PGV, and PGD, being the fundamental ground motion parameters, are much more intuitive to an engineer than SA at 0.2 or 1 s. Another reason for using PGA, PGV, and PGD is that this makes the selection of site-specific ground motions much easier. Hall et al. (1976) and Mohraz (1976) suggested the ranges, T < 0.33 s, 0.33 < T < 3.33 s, and T > 3.33 s for the acceleration-, velocity-, and displacement-sensitive regions. Figure 1 shows the correlations between SA at various periods and PGA, PGV, and PGD. It is seen that, for the selected set of strong ground motions, SAs are best correlated to PGA for the periods up to 0.2 s, to PGV for the periods between 0.2 and 3.0 s, and to PGD for the rest of the periods. A comparison of the outcomes indicates that the results of this study are different from and slightly lower than those obtained by Hall et al. (1976) and Malhotra (2006), due to difference in the datasets used. Here, the approach proposed by Malhotra (2006) is used. The main advantage of this approach lies in making no prior assumption for the cut-off periods.

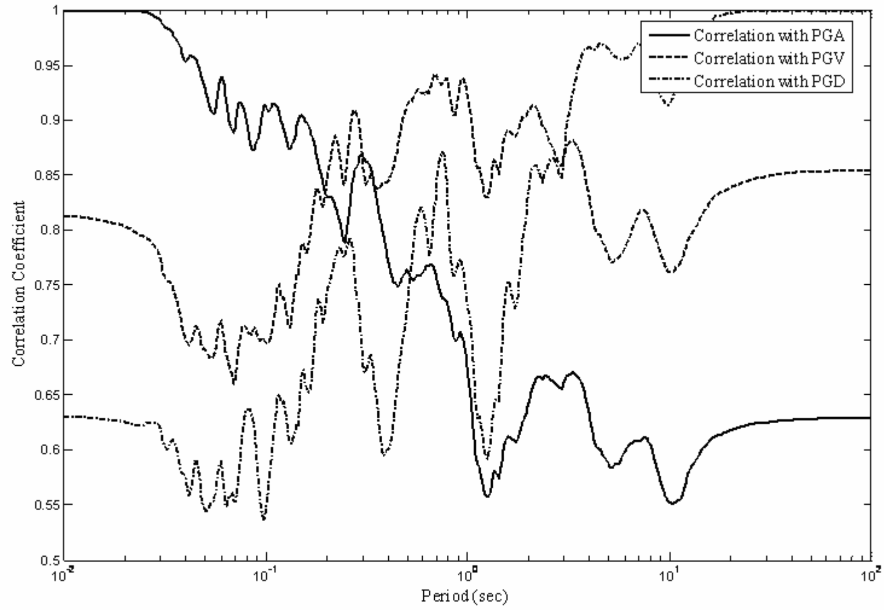

Fig. 1 Correlation of SA at various periods to peak ground motion parameters

Another issue that is not addressed in Standard No. 2800 is the evaluation of response spectrum for different damping ratios. In other words, the design spectra can be constructed only for the 5% damping. However, it is indicated that a broad range of damping ratios can be given for each type of structure, as many factors and design details have influence on the damping. In this study, a functional form of amplification factors is derived to evaluate the amplifications for any damping ratio.

The last issue addressed in this study is of smooth response spectra for the vertical component of ground motion. Conventional building structures have considerable inherent strengths in the vertical direction, and therefore, the effects of vertical components of ground motions are relatively unimportant. Probably, this is the main reason why the vertical ground motion and corresponding building factor are not included in Standard No. 2800. However, for certain types of structures (e.g., dams), the effects of vertical component may be of some significance (Chopra, 1966). In this study, a smooth response spectrum for the vertical ground motions is proposed. In addition, the corresponding amplification factors for the vertical component are also provided for different damping values.

THE ACCELEROMETRIC DATA BANK

Most of the high-populated cities in Iran are close to active faults and have been severely damaged during past moderate-to-large earthquakes. Such vulnerability to earthquakes is also evident in other historical reports. However, strong ground motions could be registered only after the installation of Iranian Strong Motion Network (ISMN) in 1973. Since 1973, the network has gradually been expanded, and at present it consists of 1065 digital and 29 analog accelerographs. Considering the locations of the severely affected regions as well as the magnitudes of the past destructive earthquakes, a set of strong-motion records, located at the near-field regions during the earthquakes with moment magnitudes equal to or larger than 6, is selected for this study. To consider the effects of strong motions, only those records for which the maximum horizontal ground accelerations are greater than 0.05g are used. The locations of stations and the corresponding seismological information for each record are given in Appendix. The geographical distribution of the stations and epicenters of the earthquakes are shown in Figure 2. The assigned site classes, based on Zare et al. (1999) and Sineian (2006), for each station are also listed in Appendix. In these studies priority is given to Vs30 and surface geology data, whenever available. Those stations, for which these parameters were not available, are classified by estimating the fundamental frequency at each station, by using Nakamura's technique. However, as it is clear from the recent studies, the site classification based on an empirical scheme should be used with care, and it should be noted that the accuracy may decrease rapidly as the number of records decreases (Zhao et al., 2006; Ghasemi et al., 2009).

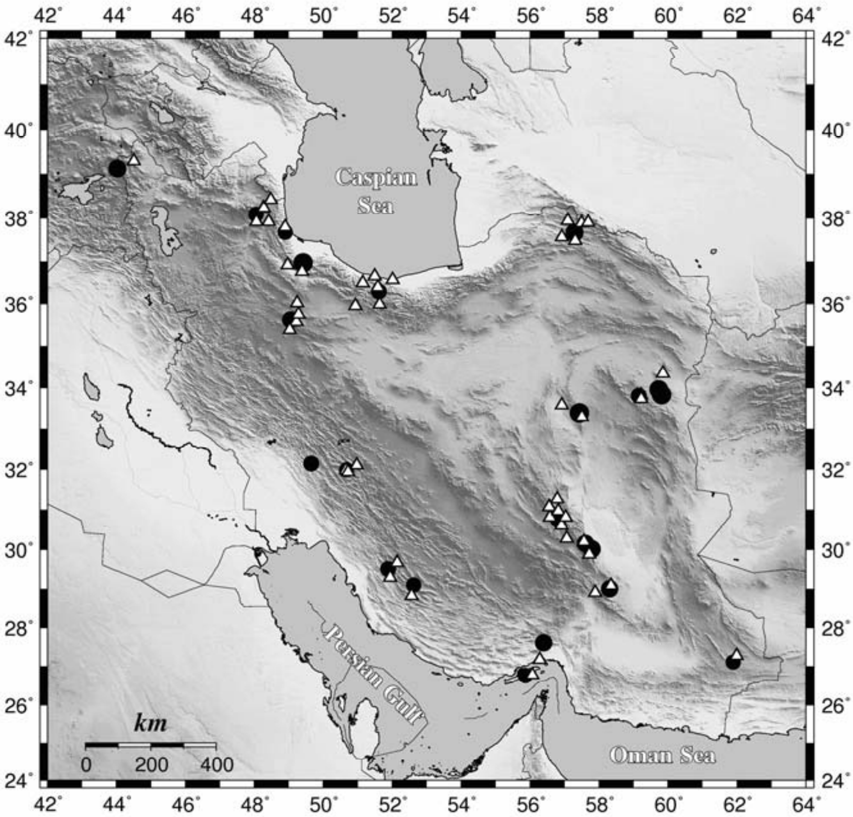

Fig. 2 The geographical distribution of the strong-motion stations (shown as triangles) and epicenters of the events (shown as circles) considered in this study

Almost all strong-motion records in the datasets show clear baseline shifts, and the records are contaminated by long-period as well as high-frequency noise. The reasons of such shifts were well addressed in the previous studies (e.g., Boore and Bommer, 2005). In this study, the procedure proposed by Boore et al. (2002) and Boore and Bommer (2005) is followed. The scheme involves fitting a quadratic polynomial to the velocity baseline followed by filtering. The processed accelerogram and the corresponding velocity and displacement time-histories for the records recorded at Bam station during the Bam earthquake of 2003 are shown in Figure 3(a). The peak ground motion parameters, PGA, PGV, and PGD, and the significant durations of strong-motion records, as considered in this study, are tabulated in Table 2. The listed PGA, PGV, and PGD are the geometric mean values of the two horizontal components, and the duration values are the averages of the significant durations in two horizontal directions. The compatible response spectrum of each component is then calculated using the methodology described in Malhotra (2001). In this method, the short-, medium-, and long-period spectral values are derived from the processed acceleration, velocity, and displacement histories, respectively. This method guarantees the correct asymptotic behavior of the computed response spectrum. Figure 3(b) demonstrates the computed response spectra, of different damping values, from the time-histories shown in Figure 3(a). In this figure all spectral quantities, like displacement, velocity, and acceleration, are displayed in a single graph (on log-log scale), known as the tripartite graph. As can be seen, the response spectrum shows the correct asymptotic behavior, i.e., the spectral acceleration approaches PGA at the short periods and the spectral deformation approaches PGD at the long periods.

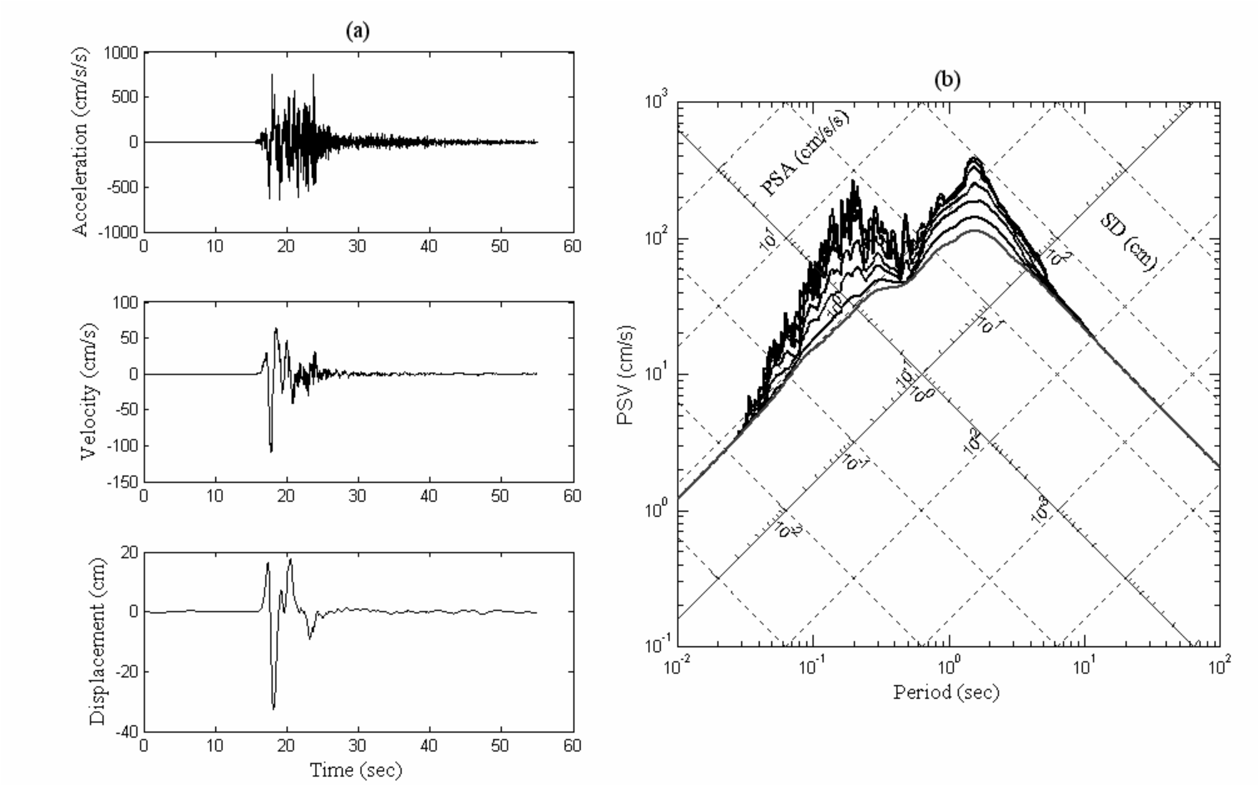

Fig. 3 (a) Processed acceleration, velocity, and displacement time-histories of the ground motion registered during the 2003 Bam earthquake at the Bam station; (b) Response spectra for several damping values computed from the time-histories at the Bam station

Table 2: Corresponding Peak Ground Motion Parameters, Significant Duration T_{cg}, and Normalized Peak Ground Velocity, of Strong-Motion Records Considered in This Study

Station	PGA (cm/s/s)	PGV (cm/s)	PGD (cm)	Duration (s)	T_{cg} (s)	$\overline{\text{PGV}}$
Kariq	541.74	14.28	0.80	4.83	0.24	0.69
Vendik	519.29	7.98	0.87	0.12	0.26	0.38
Naghan-1	81.62	2.23	0.19	0.63	0.30	0.57
Avaj	438.98	20.49	1.54	6.41	0.37	0.79
Hasan Keyf	650.28	40.28	3.23	2.18	0.44	0.88
Baraqan	93.01	3.76	0.59	9.68	0.50	0.51
Namin	89.25	2.27	0.59	13.13	0.51	0.31
Razan	193.60	9.39	1.38	13.55	0.53	0.57
Garmabdar	70.68	3.14	0.55	11.95	0.55	0.50
Poul	213.45	7.75	1.81	13.85	0.58	0.39
Shirinrood Dam1	305.84	16.71	2.70	9.28	0.59	0.58
Manjil	434.84	10.38	4.10	1.76	0.61	0.25
Sib Sooran	86.88	5.83	0.83	6.37	0.61	0.69
Suza	265.07	10.61	2.56	7.41	0.62	0.41
Balaadeh	343.32	11.58	3.41	7.61	0.63	0.34
Qasem Abad	164.93	11.93	1.93	4.78	0.68	0.67

Talesh	53.32	1.99	0.72	2.22	0.73	0.32
Khan Zeynioun	140.76	9.28	2.02	13.34	0.75	0.55
Qadrooni Dam	170.01	12.68	2.95	14.14	0.83	0.57
Deyhuk	343.01	23.32	6.55	34.25	0.87	0.49
Bojnoord	155.96	8.42	3.06	6.05	0.88	0.39
Abgarm	128.47	10.75	2.83	13.30	0.93	0.56
Naghan-1	669.47	43.45	14.89	3.06	0.94	0.44
Ravar	89.10	7.68	2.10	20.49	0.96	0.56
Dastgerd	97.62	3.30	2.39	4.80	0.98	0.22
Darsejin	63.66	3.54	1.60	12.61	0.99	0.35
Noor	56.09	6.95	1.53	28.34	1.04	0.75
Raz	88.12	5.42	2.41	14.11	1.04	0.37
Maku	83.56	3.94	2.33	18.39	1.05	0.28
Ashkhaneh	106.58	7.23	3.00	23.15	1.05	0.40
Kerman	98.95	8.66	2.94	20.32	1.08	0.51
Ghaen	168.53	14.33	5.01	10.31	1.08	0.49
Sirch	564.89	76.02	17.68	5.88	1.11	0.76
Chatrood	68.39	5.44	2.18	13.69	1.12	0.45
Helabad	67.98	5.95	2.19	12.02	1.13	0.49
Noshahr	85.75	9.19	2.84	26.07	1.14	0.59
Bam1	659.03	81.85	22.26	8.85	1.15	0.68
Zarand	268.95	24.05	9.12	18.87	1.16	0.49
Mohammad Abad-e-Maskoon	88.72	6.24	3.13	18.24	1.18	0.37
Ardebil 2	142.63	14.37	5.13	34.82	1.19	0.53
Robat	117.33	9.91	4.43	14.80	1.22	0.43
Bandarabbas	129.56	11.35	4.98	22.32	1.23	0.45
Gifan	136.40	9.70	5.25	14.69	1.23	0.36
Abbar	568.93	46.48	22.16	30.14	1.24	0.41
Golbaf	250.28	27.18	10.16	38.64	1.27	0.54
Dasht-e-Khak	52.88	4.60	2.27	14.58	1.30	0.42
Ardebil 1	95.92	9.22	4.53	34.12	1.36	0.44
Ghaen	173.44	16.04	9.30	12.74	1.45	0.40
Tabas	852.93	94.05	52.60	18.86	1.56	0.44
Firouzabad	105.73	10.90	8.75	10.37	1.81	0.36

RELATIONSHIPS BETWEEN PEAK GROUND MOTION PARAMETERS

The seismic macrozonation hazard map in Standard No. 2800 suggests only the base acceleration values for the zones with different hazard levels; however, as mentioned before, to construct a design response spectrum, PGV and PGD estimates are also needed. Mohraz (1976) and Hall et al. (1976) used two different ratios to estimate PGV and PGD from the specified design acceleration. These ratios are PGV to PGA ratio, called as v/a ratio, and PGA-PGD product to PGV-squared ratio, called as ad/v^2 ratio; the latter ratio represents the frequency bandwidth of the ground motion. For each site category, Mohraz (1976) considered the horizontal components with larger and smaller peak ground accelerations and the vertical components of records as separate groups. The desired ratios were then derived statistically for the individual groups. In this study, strong-motion records are also grouped according to this criterion. Figure 4 shows box and whisker plots for v/a and ad/v^2 ratios for each site category; the boxes have lines at the lower, median, and upper quartile values, while the whiskers are the lines extending from each end of the box to show the extent of the rest of the data. The ratios shown in the figure are computed from the horizontal components of records with larger peak ground accelerations. For 50 percentile, the v/a values are 0.054, 0.039, 0.082, and 0.075 s for the SC-I, SC-II, SC-III, and SC-IV sites, respectively. Generally, the rock sites (i.e., SC-I sites) show lower v/a values than the soil sites (i.e., SC-III, SC-IV sites), which indicates a shift toward the longer-period motions on softer soil sites. The corresponding values for the ad/v^2 ratio are 5.53, 5.51, 4.33, and 4.20. The highest value is obtained, on average, for the rock sites, indicating that the average spectrum for such sites has a broader bandwidth.

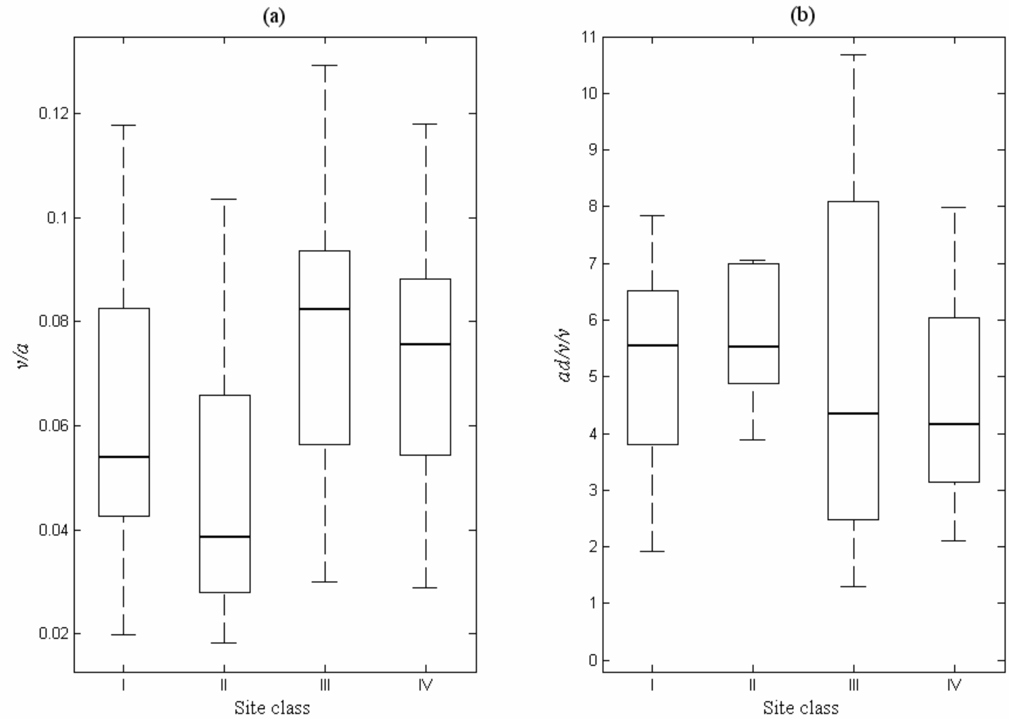

Fig. 4 Box and whisker plots for the (a) v/a and (b) ad/v^2 ratio, for each site category

Although the strong-motion records are grouped according to the criterion of Mohraz (1976), the consequences of a balanced one-way analysis of variance indicate that the results for the horizontal components of records with larger peak ground accelerations are not significantly different from those with smaller peak ground accelerations. The same conclusion can be made for the ratios calculated for each site condition. Therefore, only one set of the desired ratios for the horizontal and vertical components is proposed in this paper. The 50 and 84.1 percentile values for the v/a and ad/v^2 ratios are tabulated in Table 3. The median and median plus one standard deviation of the peak vertical to peak horizontal acceleration ratio are 0.6 and 0.9, respectively. For engineering purposes, the peak vertical acceleration is often assumed to be two-third of the peak horizontal one, which is slightly less than the 84.1 percentile and higher than the median values obtained in this study.

Table 3: 50 and 84.1 Percentiles of the v/a and ad/v^2 Ratios for Horizontal and Vertical Ground Motions

Component	v/a (s)		ad/v^2	
	Percentile		Percentile	
	50	84.1	50	84.1
Horizontal	0.068	0.1	4.8	8.3
Vertical	0.067	0.1	5.8	9.7

It is important to bear in mind that the relationships between PGA and PGV and between PGA and PGD depend on the magnitude of the earthquake and the distance of the site from the source; hence, in practice, the three peak ground motion parameters should be estimated independently.

SMOOTH SPECTRUM OF GROUND MOTIONS

Different response spectra, as calculated from different strong-motion records, can be compared by normalizing those to the same scale. The normalization involves defining cutoff periods for the acceleration-, velocity- and displacement-sensitive regions, and then dividing the spectral values at each period to the corresponding peak ground motion parameter. However, such a scheme needs a prior assumption of the cutoff periods (Newmark and Hall, 1982; Hall et al., 1976; Mohraz, 1976), which can change from one set of ground motions to another. In this study, the normalization scheme proposed by Malhotra (2006) is followed. This scheme has an advantage that it needs no prior assumption of the cutoff periods. It involves normalization of the period scale by dividing all periods by

$$T_{cg} = 2\pi\sqrt{\frac{\mathrm{PGD}}{\mathrm{PGA}}} \tag{2}$$

where T_{cg} marks the boundary between the high- and low-frequency regions (Malhotra, 2001, 2006). Next, the spectral velocity (SV) and PGV are normalized by the $\sqrt{\mathrm{PGA}\times\mathrm{PGD}}$ factor.

Normalized peak ground velocity, $\overline{\mathrm{PGV}}$, is related to the reciprocal of ad/v^2 ratio, and hence, higher values of normalized peak ground velocity are generally expected for the ground motions on softer soil sites. This implies that the ground motions on soil sites have narrower bandwidths. The values of T_{cg} and normalized peak ground velocity of the records considered in this study are listed in Table 2. The reported values are geometric means of the two horizontal components. Figure 5 shows the normalized 5%-damping response spectra of the horizontal and vertical components of ground motions included in the data bank. The values of T_{cg} for the horizontal ground motions range from 0.2 to 2.2 s; similar ranges are obtained for the vertical ground motions. However, Malhotra (2006) obtained shorter values of T_{cg} for the vertical ground motions than those for the horizontal ones. The similarities between the central periods of vertical and horizontal motions, as observed in this study, could be due to the closeness of the sites of all records (selected for this study) to the sources of events. Therefore, vertical motions are comparable to the horizontal ones in high and low frequencies. The median values of normalized peak ground velocities for the horizontal and vertical ground motions are 0.46 and 0.4, respectively. As the normalized peak ground velocity is a measure of the spectral width, lower values for the vertical motions in comparison with the horizontal ones implies that the average spectrum of vertical motions is flatter than that of the horizontal ones. The normalized 5%-damping median spectra of the horizontal and vertical ground motions in the data bank are shown in Figure 6. The shaded area in this figure corresponds to ± 1 standard deviation about the median. Idealized forms of the normalized median spectra for different damping values are shown in Figure 7. As expected, the spectra of vertical motions are flatter than those of the horizontal ones, and the amplification factors decrease with an increase in the damping value. The acceleration, velocity, and displacement amplification factors, α_A, α_V, and α_D, respectively, for the median horizontal and vertical spectra of different damping ratios are listed in Table 4. The amplification factors for different site conditions are also calculated; however, the differences between different site conditions are statistically insignificant according to the variance analysis. The horizontal amplification factors obtained in this study are compared with those reported by Mohraz (1976), Newmark and Hall (1982), and Malhotra (2006), as shown in Figure 8. The α_A values obtained in this study are up to about 10% higher in comparison with those reported by Mohraz (1976), 13% higher as compared to those given by Newmark and Hall (1982), and 3% higher than the values reported by Malhotra (2006). Similarly, the α_V values are about 10% higher than the values reported by Mohraz (1976), 28% lower than those reported by Newmark and Hall (1982), and 18% lower than those given by Malhotra (2006). Further, the α_D values are up to about 4% higher than those given by Mohraz (1976), 23% higher than those reported by Newmark and Hall (1982), and 4% lower than those given by

Malhotra (2006). The present results for α_A and α_D factors are mostly consistent with those obtained by Malhotra (2006), and for α_V values with those of Mohraz (1976). Malhotra (2006) considers the prior assumption of cutoff periods in the studies of Mohraz (1976) and Newmark and Hall (1969, 1982) as the possible source of differences between the calculated amplification factors. The functional form of amplification factors considered in this study is

$$\alpha(\xi) = a + b \ln \xi \tag{3}$$

where α denotes α_A, α_V, or α_D, and ξ denotes the percentage of critical damping. The coefficients, a and b, in Equation (3) are determined through least-squares fitting of the data points in Table 4 and are given in Table 5. The higher-order terms have been considered in Equation (3) elsewhere (e.g., see Malhotra, 2006); however, the coefficients for such terms seem to be statistically insignificant.

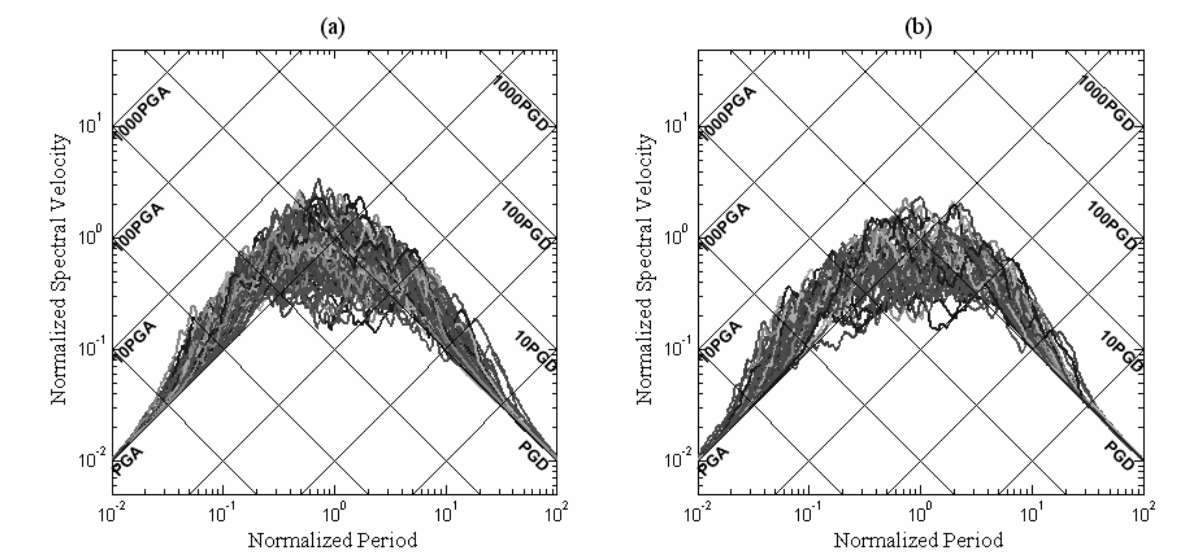

Fig. 5 Normalized 5%-damping response spectra of (a) horizontal and (b) vertical components

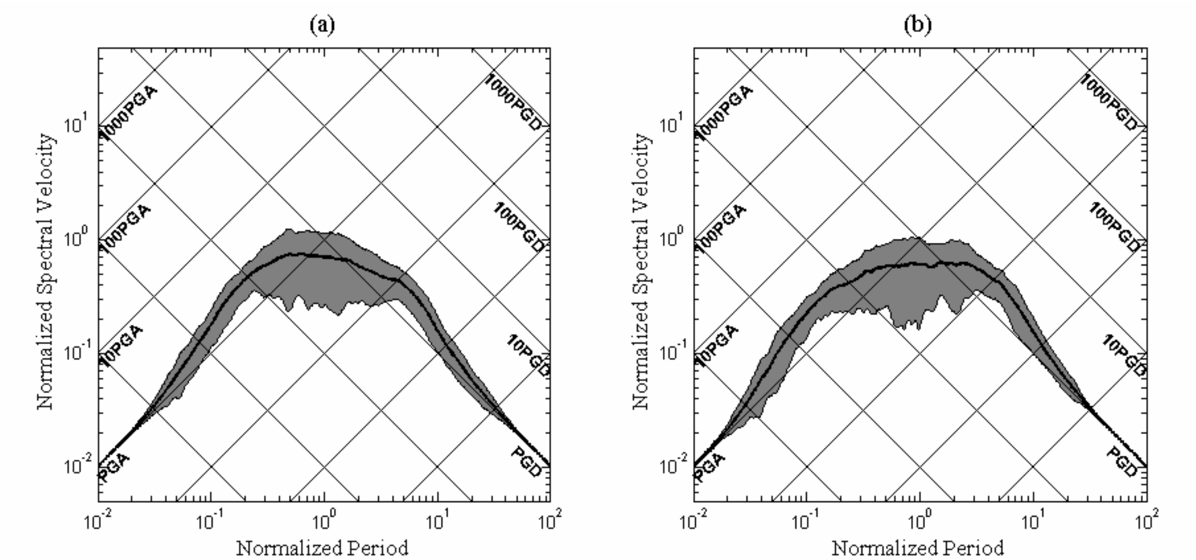

Fig. 6 Normalized 5%-damping median spectra of (a) horizontal and (b) vertical ground motions (the shaded area corresponds to ± 1 standard deviation about the median)

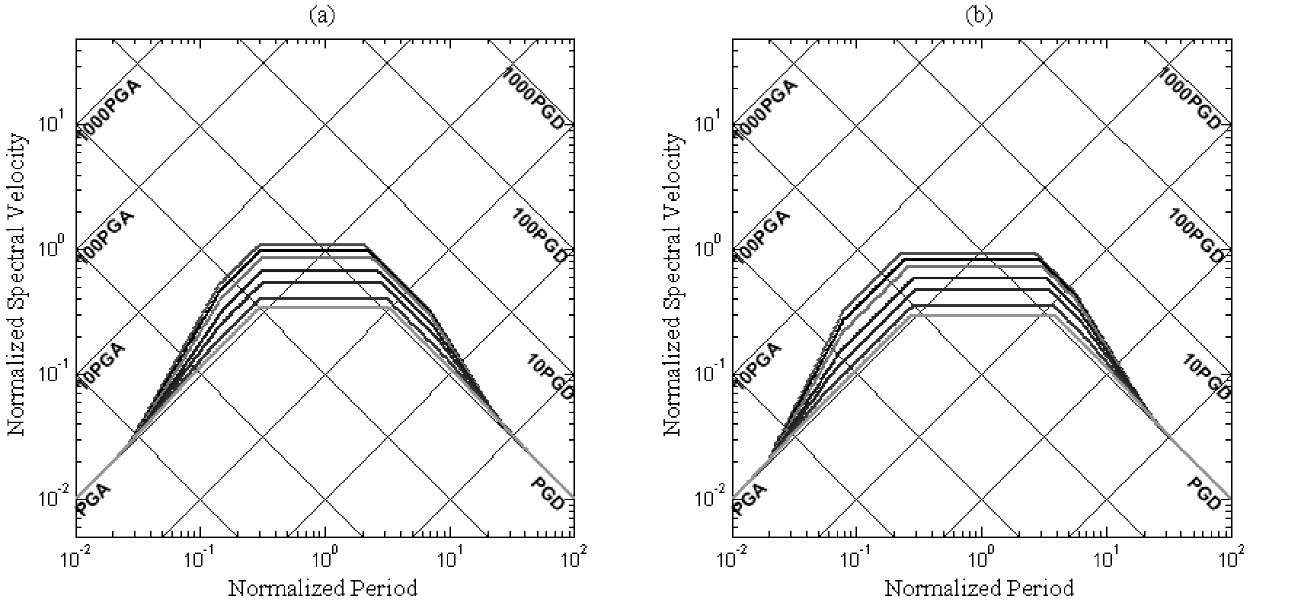

Fig. 7 Idealized forms of the normalized median spectra for different damping values in (a) horizontal and (b) vertical component

Table 4: Acceleration, Velocity and Displacement Amplification Factors for the Median Horizontal and Vertical Spectra of Different Damping Ratios

Damping Ratio (%)	Horizontal			Vertical		
	α_A	α_V	α_D	α_A	α_V	α_D
0.5	3.70	2.22	2.26	4.16	2.18	2.53
1	3.25	2.00	2.19	3.47	1.98	2.43
2	2.78	1.75	2.06	2.83	1.74	2.27
5	2.17	1.38	1.80	2.09	1.39	1.98
10	1.74	1.10	1.54	1.63	1.11	1.67
20	1.35	0.84	1.26	1.27	0.85	1.34
30	1.16	0.70	1.11	1.10	0.70	1.15

The procedure for constructing a smooth response spectrum at the site of interest consists of (a) first estimating three peak ground motion parameters (i.e., PGA, PGV, and PGD) and three amplification factors for the acceleration-, velocity- and displacement-sensitive regions at the site, and (b) then obtaining the spectrum ordinates in each region from the product of the relevant ground motion parameter and its amplification factor. Generally, PGA, PGV, and PGD can be determined by using the results of SHA studies in the region. The amplification factors for the specified damping value can be obtained by using Table 4.

In this study, following the procedure described above, the smooth spectra of numerous horizontal and vertical ground motions are computed via their corresponding peak ground motion parameters. The spectral ordinates for these ground motions are calculated by the method suggested by Malhotra (2006), and the results are presented in this study. In order to validate the results, as obtained by analyzing the Iranian strong-motion records, the ratio between the smoothed and actual response spectra is calculated for each ground motion. Figure 9 shows the median spectral ratio for horizontal and vertical ground motions; the shaded area corresponds to ± 1 standard deviation about the median. The closeness of the median ratio of actual and smoothed SVs to unity for all natural periods confirms accuracy of the results obtained in this study. Here, a t-test of the hypothesis is also performed, i.e., the data points in each period range come from a united distribution. The results indicate that the null hypothesis cannot be rejected in wide period ranges.

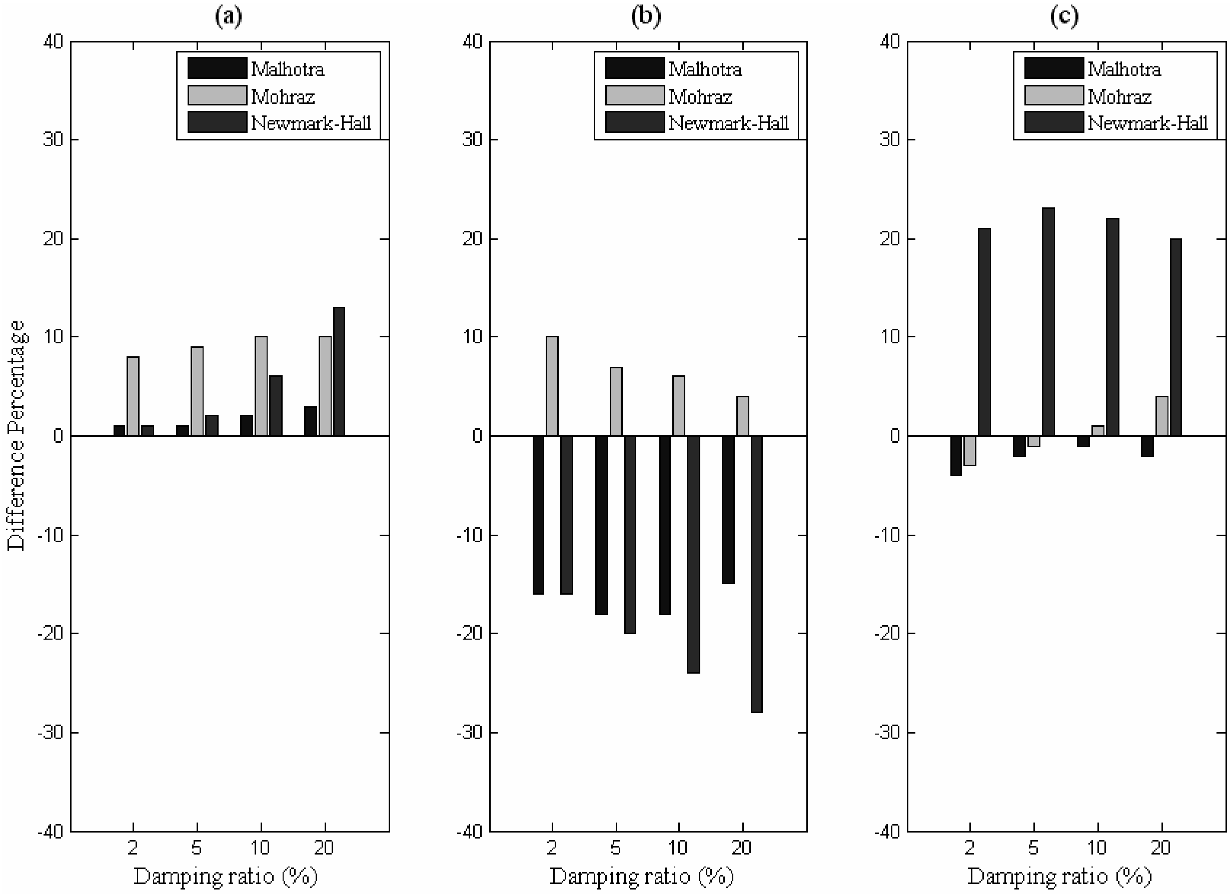

Fig. 8 Comparison between the amplification factors obtained in this study and those suggested by the previous ones: (a) acceleration, (b) velocity, (c) displacement (the values obtained here are shown in the form of percentage differences from the previous studies)

Table 5: Functional Form of the Amplification Factors for Horizontal and Vertical Spectra

	Horizontal	Vertical
α_A	$-0.628\ln\xi + 3.233$	$-0.748\ln\xi + 3.466$
α_V	$-0.379\ln\xi + 1.985$	$-0.368\ln\xi + 1.964$
α_D	$-0.291\ln\xi + 2.175$	$-0.345\ln\xi + 2.419$

AN EXAMPLE ON CONSTRUCTING SMOOTH RESPONSE SPECTRA

Here, the construction of smooth design spectrum using peak ground motion parameters is presented in an example. Based on the seismic hazard map prepared for the Tehran metropolitan (Zare, 2004), the expected PGA value is 0.45g (441 cm/s/s) for a 475-year return period. The PGV and PGD values are 30 cm/s and 9.8 cm, respectively. To construct the smooth spectrum for 5% damping and for horizontal component, the desired amplification factors are obtained from Table 3, and the control periods which are the beginning and end points of the acceleration-, velocity- and displacement-sensitive regions, are computed as follows:

$$T_3 = 2\pi\frac{\mathrm{PGV}\times\alpha_V}{\mathrm{PGA}\times\alpha_A} = 2\pi\frac{30\times1.38}{411\times2.17} = 0.29\,\mathrm{s} \tag{3}$$

$$T_4 = 2\pi\frac{\mathrm{PGD}\times\alpha_D}{\mathrm{PGV}\times\alpha_V} = 2\pi\frac{9.8\times1.8}{30\times1.38} = 2.7\,\mathrm{s} \tag{4}$$

$$T_1 = \frac{T_3}{10.8} = \frac{0.29}{10.8} = 0.026\,\text{s} \tag{5}$$

$$T_2 = \frac{T_3}{2} = \frac{0.29}{2} = 0.14\,\text{s} \tag{6}$$

$$T_5 = 2.7T_4 = 2.7 \times 2.7 = 7.3\,\text{s} \tag{7}$$

$$T_6 = 10.8T_4 = 10.8 \times 2.7 = 29.16\,\text{s} \tag{8}$$

The desired smooth spectrum can be drawn on a tripartite paper (see Figure 10) as follows. Take SA = PGA for $T < T_1$ and SA = α_A ×PGA for $T_2 < T < T_3$. Join SA(T_1) = PGA and SA(T_2) = α_A ×PGA by a straight line. Take SV = α_V ×PGV for $T_3 < T < T_4$, SD = PGD for $T > T_6$, and SD = α_D ×PGD for $T_4 < T < T_5$. Join SD(T_6) = PGD and SD(T_5) = α_D ×PGD by a straight line.

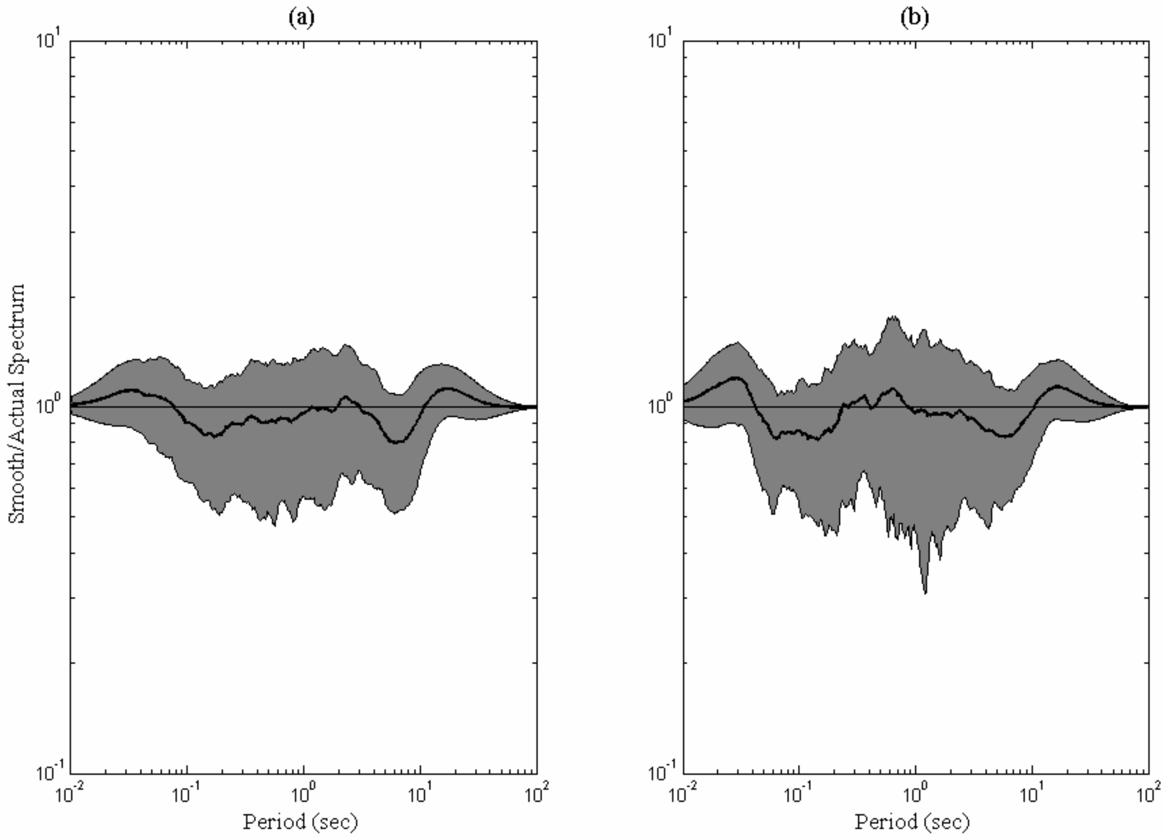

Fig. 9 Median ratios between the 5%-damping smooth spectrum and the actual spectra of (a) horizontal and (b) vertical ground motions (the shaded area corresponds to ± 1 standard deviation about the median)

Such a smooth response spectrum characterizes the earthquake loading and can be used in a pseudo-static analysis, which is needed for a majority of structures. However, for some specific design situations a suite of strong-motion records is required for input into the time-domain nonlinear analysis of structures. These time-histories can be selected from a data bank of real accelerograms; however, the selected ground motion records should be modified to be compatible with the seismic hazard level determined for the target region. Such a modification can be applied by scaling and stretching the selected time-histories. Scaling, which is the multiplication of the accelerogram by a scale factor, makes the peak value of the accelerogram (e.g., PGA) equal to the design value. Hence, scaling affects only the PGA, not T_{cg} and the normalized velocity. In contrast, stretching accelerograms along the time axis changes the duration of the record and frequency content and can be used to change T_{cg}. In practice, it is desirable to combine the scaling-stretching technique to match the PGA, PGV, and PGD with the target values.

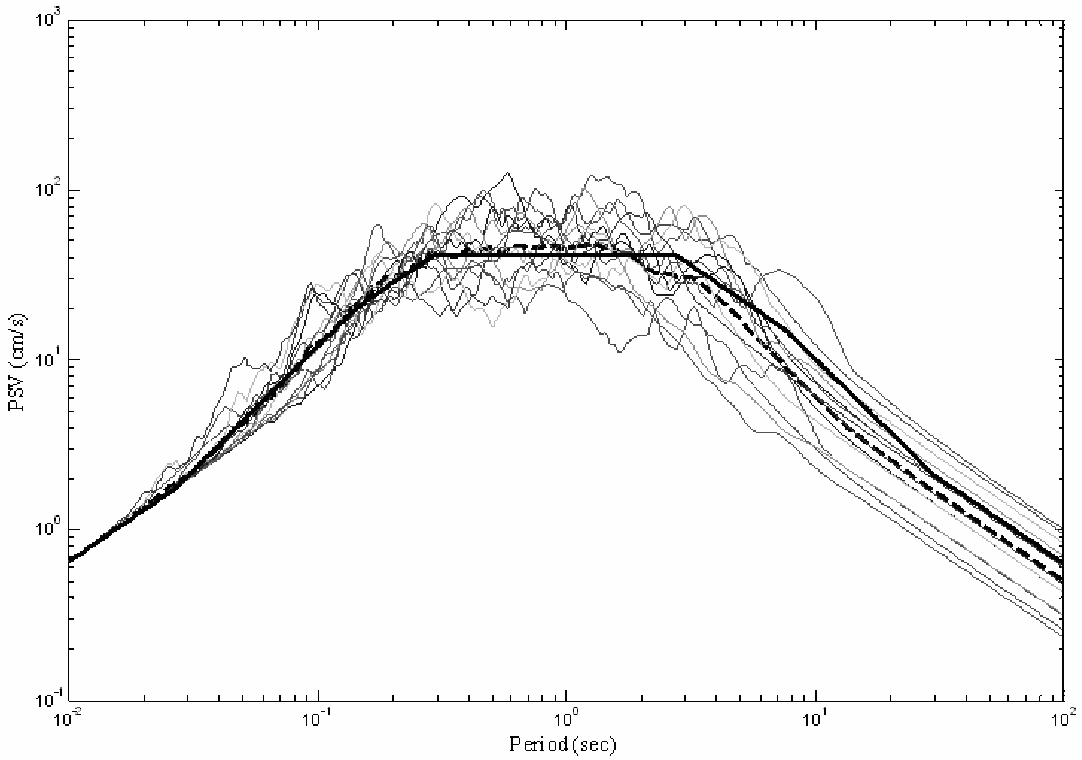

Fig. 10 5%-damping response spectra (in thin lines) of the scaled accelerograms selected to derive design spectra in the Tehran region (the black dotted curve is the geometric-mean spectrum; the black thick curve is the smooth design spectrum calculated using the procedure described in this study)

In the above example, based on the calculated PGA, PGV and PGD for the Tehran region, six time histories are selected that have peak ground motion parameters close to these values. The selected accelerograms are scaled and stretched to meet the demand at the site. Figure 11 shows the horizontal component of the ground motion recorded at the Zarand station during the Zarand earthquake of 2005 as well as the corresponding scaled and stretched time-histories. The PGA of the scaled and stretched accelerogram exactly matches the target value, and the corresponding PGV and PGD values are close to the target ones. In fact, PGA should be matched exactly in the stiff structures, PGV in the moderately stiff structures, and PGD in the flexible structures. The 5%-damping geometric mean spectrum of the selected time-histories is shown in Figure 10. It can be seen that the proposed smooth spectrum for the Tehran region, as obtained by using the described procedure, is consistent with the one determined based on the strong-motion records.

CONCLUDING REMARKS

This study summarizes the results of a comprehensive statistical study on constructing smooth response spectra in Iran. A total of 51 Iranian near-field (three-component) strong-motion records, recorded during 10 moderate-to-large earthquakes, are considered in this study. The main reason for focusing on Iranian plateau is because this region is one of the most seismically active regions in the world, and also has considerable number of strong-motion records which can be used to propose region-specific smooth response spectra. The near-field records are used mainly because of the fact that most of the high-populated cities in Iran are located in the near-field regions. The following conclusions are drawn from the results obtained in this study:

1. The cutoff periods for each region are slightly lower than the values reported in Mohraz (1976) and Malhotra (2006), indicating that those can change from one set of ground motions to another.
2. The ratio of velocity to acceleration and that of acceleration-displacement product to velocity squared are calculated to state the relationships between the peak ground motion parameters.
3. Generally, SC-I sites show lower v/a values and higher ad/v^2 values than the other site categories. This is consistent with the results obtained by Mohraz (1976) and Malhotra (2006).

4. The results of analysis of variance indicate that the differences between the ratios obtained at different site categories are statistically insignificant.
5. The amplification factors for the median horizontal and vertical spectra of different damping ratios are calculated and compared with the results obtained in the previous studies. The amplification factors, α_A and α_D, as obtained in this study are mostly consistent with those obtained by Malhotra (2006), and the α_V values are consistent with the results obtained by Mohraz (1976).
6. The amplification factors for the median horizontal and vertical spectra of different damping ratios are close together, however, the shape of the median vertical spectrum is much flatter than the horizontal one.
7. The results of analysis of variance indicate that the differences between the amplification factors obtained at different site categories are statistically insignificant.
8. In this study, no significant statistical difference is obtained between the desired parameters for different site conditions, which might be due to errors in the initial assignment of site classes. Site classes are initially assigned by using the empirical classification schemes. However, the results from the recent studies indicate that the accuracy of such empirical schemes may decrease rapidly with a decreasing number of records at each station.
9. The comparison between the smoothed and actual response spectra for the horizontal and vertical components validates the results of this study.
10. The smooth response spectrum, as constructed by using the procedure proposed in this study, is consistent with the mean response spectrum, which has been computed based on the response spectra of the accelerograms of the ISMN data bank.
11. The results of this study are effective in the evaluation of the present Iranian seismic code and can be used directly in future SHA projects in Iran. This study could be used as the basis for a more comprehensive study in developing the design response spectra by increasing the number of strong motions in the accelerometric data bank and by discussions on standard deviations in the spectral amplitudes in very low and very long periods.

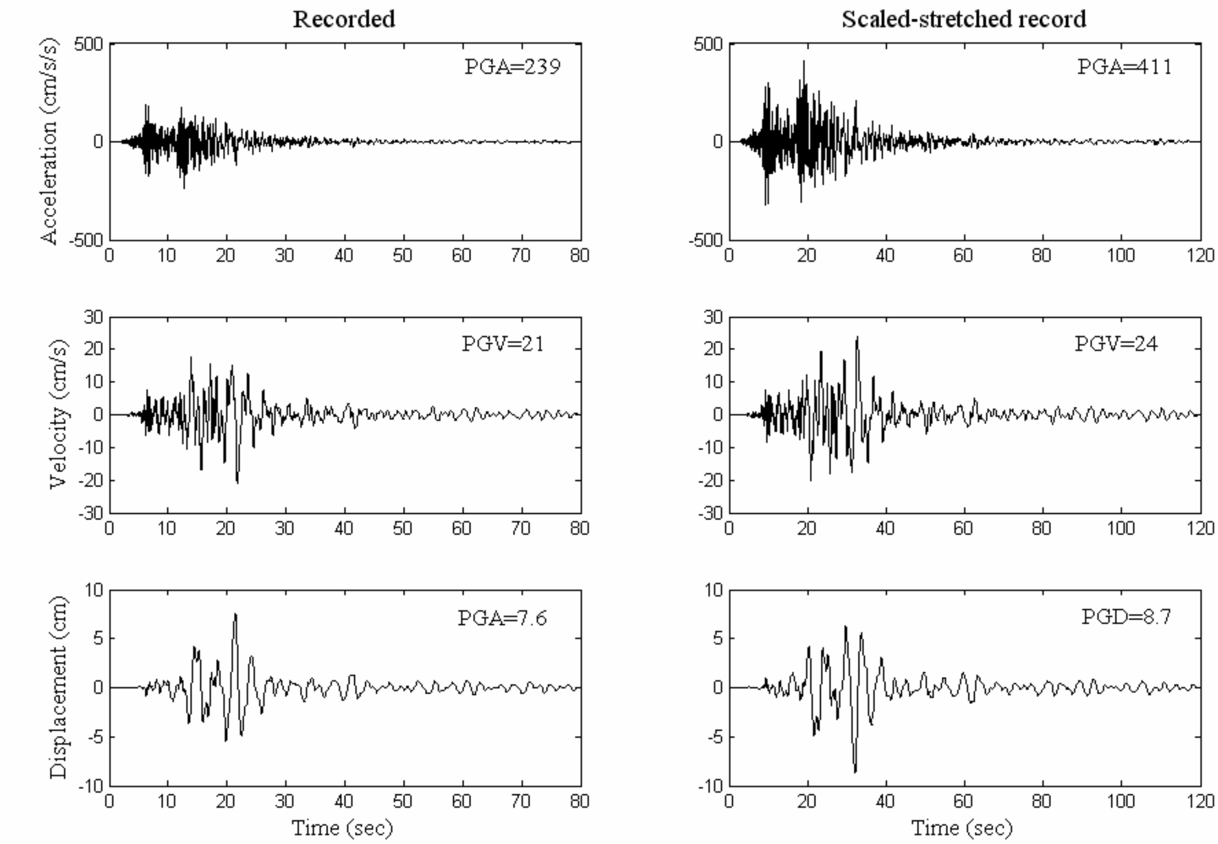

Fig. 11 Acceleration, velocity and displacement time-histories of the Zarand earthquake of 2005, as recorded at the Zarand station, and the corresponding scaled and stretched time-histories

ACKNOWLEDGEMENTS

We are very thankful to the three anonymous reviewers for their constructive comments on the first version of this manuscript. We are also thankful to Dr. Praveen K. Malhotra from FM Global, USA for his support and encouragement during this study. We thank Building and Housing Research Center (BHRC) for making the strong-motion records available.

APPENDIX: LOCATIONS OF RECORDING STATIONS, ASSIGNED SITE CLASSES, AND CORRESPONDING SEISMOLOGICAL INFORMATION

No.	Station	Lat.	Long.	Site Class	Date	M_w	R (km)
1	Vendik	33.82	59.23	II	11/7/1976	6.4	11
2	Ghaen	33.73	59.22	I	11/7/1976	6.4	10
3	Maku	39.29	44.51	II	11/24/1976	7.3	48
4	Bandarabbas	27.18	56.28	II	3/21/1977	7.0	52
5	Naghan-1	31.93	50.72	I	4/6/1977	6.1	7
6	Dastgerd	32.10	50.98	II	4/6/1977	6.1	18
7	Ardal	31.98	50.66	IV	4/6/1977	6.1	21
8	Deyhuk	33.29	57.50	I	9/16/1978	7.4	36
9	Tabas	33.58	56.92	I	9/16/1978	7.4	27
10	Talesh	37.80	48.90	III	11/4/1978	6.2	20
11	Naghan-1	31.93	50.72	I	12/14/1978	6.1	5
12	Ghaen	33.73	59.22	I	11/27/1979	7.1	44
13	Golbaf	29.88	57.72	III	7/28/1981	7.1	12
14	Kerman	30.28	57.07	IV	7/28/1981	7.1	48
15	Abbar	36.92	48.97	I	6/20/1990	7.3	40
16	Manjil	36.76	49.39	II	6/20/1990	7.3	12
17	Firouzabad	28.83	52.56	III	3/1/1994	6.0	31
18	Bojnoord	37.48	57.31	III	2/4/1997	6.5	10
19	Gifan	37.89	57.49	IV	2/4/1997	6.5	29
20	Ashkhaneh	37.56	56.92	III	2/4/1997	6.5	56
21	Robat	37.90	57.69	IV	2/4/1997	6.5	41
22	Raz	37.94	57.10	III	2/4/1997	6.5	42
23	Kariq	37.92	48.06	II	2/28/1997	6.1	26
24	Ardebil 2	38.22	48.26	III	2/28/1997	6.1	37
25	Ardebil 1	38.23	48.28	I	2/28/1997	6.1	37
26	Namin	38.42	48.48	II	2/28/1997	6.1	58
27	Helabad	37.92	48.42	IV	2/28/1997	6.1	37
28	Qasem Abad	34.35	59.86	IV	5/10/1997	7.1	55
29	Sirch	30.20	57.56	III	3/14/1998	6.3	12
30	Balaadeh	29.29	51.94	I	5/6/1999	6.2	49
31	Khan zeynioun	29.67	52.15	I	5/6/1999	6.2	30
32	Avaj	35.58	49.22	I	6/22/2002	6.4	30
33	Razan	35.39	49.03	IV	6/22/2002	6.4	34
34	Abgarm	35.76	49.28	IV	6/22/2002	6.4	37

35	Darsejin	36.02	49.24	II	6/22/2002	6.4	38
36	Bam1	29.09	58.35	III	12/26/2003	6.5	9
37	Mohammad Abad-e-Maskoon	28.91	57.89	II	12/26/2003	6.5	59
38	Hasan Keyf	36.5	51.15	III	5/28/2004	6.3	43
39	Poul	36.401	51.586	IV	5/28/2004	6.3	17
40	Baraqan	35.953	50.935		5/28/2004	6.3	69
41	Noshahr	36.654	51.494	IV	5/28/2004	6.3	39
42	Garmabdar	35.987	51.634		5/28/2004	6.3	35
43	Noor	36.574	52.011	IV	5/28/2004	6.3	51
44	Chatrood	30.605	56.911	II	2/22/2005	6.2	36
45	Ravar	31.263	56.791	III	2/22/2005	6.2	66
46	Zarand	30.81	56.577	III	2/22/2005	6.2	40
47	Dasht-e-Khak	31.066	56.555	IV	2/22/2005	6.2	36
48	Qadrooni Dam	30.962	56.819	IV	2/22/2005	6.2	29
49	Shirinrood Dam1	30.811	57.031	II	2/22/2005	6.2	33
50	Sib Sooran	27.286	61.998		3/13/2005	6.0	53
51	Suza	26.782	56.07	I	11/27/2005	6.1	17

REFERENCES

1. BHRC (2003). "Iranian Code of Practice for Seismic Resistant Design of Buildings, Standard No. 2800", Publication No. S-374, Building & Housing Research Center, Tehran, Iran.
2. Boore, D.M. and Bommer, J.J. (2005). "Processing of Strong-Motion Accelerograms: Needs, Options and Consequences", Soil Dynamics and Earthquake Engineering, Vol. 25, No. 2, pp. 93–115.
3. Boore, D.M., Stephens, C.D. and Joyner, W.B. (2002). "Comments on Baseline Correction of Digital Strong-Motion Data: Examples from the 1999 Hector Mine, California, Earthquake", Bulletin of the Seismological Society of America, Vol. 92, No. 4, pp. 1543–1560.
4. Chopra, A.K. (1966). "The Importance of the Vertical Component of Earthquake Motions", Bulletin of the Seismological Society of America, Vol. 56, No. 5, pp. 1163–1175.
5. Ghasemi, H., Zare, M., Fukushima, Y. and Sinaeian, F. (2009). "Applying Empirical Methods in Site Classification Using Response Spectral Ratio (H/V): A Case Study on Iranian Strong Motion Network (ISMN)", Soil Dynamics and Earthquake Engineering, Vol. 29, No. 1, pp. 121–132.
6. Ghodrati Amiri, G., Zahedi, M. and Taghdir, A. (2003). "Evaluation of Soil Type Classification of the 2800 Code Based on Response Spectrum Study", Proceedings of the Third Conference on Iranian Code for Seismic Resistant Design of Buildings, Tehran, Iran, Vol. 1, pp. 111–120 (in Persian).
7. Hall, W.J., Mohraz, B. and Newmark, N.M. (1976). "Statistical Studies of Vertical and Horizontal Earthquake Spectra", Report NUREG-0003 (prepared for U.S. Nuclear Regulatory Commission, Washington, DC, U.S.A.), Nathan M. Newmark Consulting Engineering Services, Urbana, U.S.A.
8. ICC (2003). "International Building Code", International Code Council, Washington, DC, U.S.A.
9. ICC (2006). "International Building Code", International Code Council, Washington, DC, U.S.A.
10. Malhotra, P.K. (2001). "Response Spectrum of Incompatible Acceleration, Velocity and Displacement Histories", Earthquake Engineering & Structural Dynamics, Vol 30, No. 2, pp. 279–286.
11. Malhotra, P.K. (2006). "Smooth Spectra of Horizontal and Vertical Ground Motions", Bulletin of the Seismological Society of America, Vol. 96, No. 2, pp. 506–518.
12. Mohraz, B. (1976). "A Study of Earthquake Response Spectra for Different Geological Conditions", Bulletin of the Seismological Society of America, Vol. 66, No. 3, pp. 915–935.

13. Mohraz, B., Hall, W.J. and Newmark, N.M. (1973). "A Study of Vertical and Horizontal Earthquake Spectra", Report WASH-1255 (prepared for U.S. Atomic Energy Commission, Washington, DC, U.S.A.), Nathan M. Newmark Consulting Engineering Services, Urbana, U.S.A.
14. Newmark, N.M. and Hall, W.J. (1969). "Seismic Design Criteria for Nuclear Reactor Facilities", Proceedings of the Fourth World Conference on Earthquake Engineering, Santiago, Chile, Vol. 2, pp. B-4: 37–50.
15. Newmark, N.M. and Hall, W.J. (1982). "Earthquake Spectra and Design", Earthquake Engineering Research Institute, Okland, U.S.A.
16. Sinaiean, F. (2006). "Study on Iran Strong Motion Records", Ph.D. Thesis, International Institute of Earthquake Engineering and Seismology, Tehran, Iran.
17. Tehranizadeh, M. and Hamedi, F. (2003). "Influence of Iran's Earthquake Ground Motion Parameters on Design Spectra Using Deterministic and Probabilistic Approaches", Journal of Earthquake Engineering, Vol. 7, No. 2, pp. 275–295.
18. Zare, M. (2004). "Seismic Hazard Analysis for Tehran Metropolitan", Research Report, International Institute of Earthquake Engineering and Seismology, Tehran, Iran (in Persian).
19. Zare, M., Bard, P.-Y. and Ghafory-Ashtiany, M. (1999). "Site Characterizations for the Iranian Strong Motion Network", Soil Dynamics and Earthquake Engineering, Vol. 18, No. 2, pp. 101–123.
20. Zhao, J.X., Irikura, K., Zhang, J., Fukushima, Y., Somerville, P.G., Asano, A., Ohno, Y., Oouchi, T., Takahashi, T. and Ogawa, H. (2006). "An Empirical Site-Classification Method for Strong-Motion Stations in Japan Using H/V Response Spectral Ratio", Bulletin of the Seismological Society of America, Vol. 96, No. 3, pp. 914–925.

ISET Journal of Earthquake Technology, Paper No. 501, Vol. 46, No. 1, March 2009, pp. 19–28

ARTIFICIAL NEURAL NETWORK-BASED ESTIMATION OF PEAK GROUND ACCELERATION

C.R. Arjun and Ashok Kumar
Department of Earthquake Engineering
Indian Institute of Technology Roorkee
Roorkee-247667

ABSTRACT

This paper presents the application of artificial neural networks (ANNs) for the estimation of peak ground acceleration (PGA) for the earthquakes of magnitudes more than 5.0 and hypocentral distances less than 50 km. Earthquake magnitude, hypocentral distance, and average values of four geophysical properties of the site, i.e., standard penetration test (SPT) blow count, primary wave velocity, shear wave velocity, and density of soil, have been used as six input variables to train the neural network. An attempt has also been made to train the neural network with magnitude, hypocentral distance and average shear wave velocity as three input variables. This study shows that ANN is a valuable tool for the prediction of peak ground acceleration at a site, given the magnitude and location of earthquake, and local soil conditions. It has also been observed that the prediction using the trained network with six inputs is better than that with three inputs.

KEYWORDS: Artificial Neural Networks, Peak Ground Acceleration, Hypocentral Distance, Shear Wave Velocity

INTRODUCTION

Historically, peak ground acceleration has been considered as a parameter representing the severity of shaking at a site. Traditionally, engineers have been interested in the acceleration, which can be related to force. Peak ground acceleration (PGA), also termed as zero-period acceleration (ZPA), is defined as the absolute maximum amplitude of recorded acceleration. In the past, more than 120 equations have been derived to predict PGA (Douglas, 2003). A majority of the published ground motion estimation relations involves assumption of a model (i.e., a mathematical function) that relates a given strong-motion parameter to one or more parameters comprising magnitude, distance, and local site conditions. Subsequently, by using a strong ground motion dataset, ground motion relations are developed from the statistical regression analyses. Regression analysis is used to determine the best estimates of various constants in the mathematical function. The emergence of artificial neural networks (ANNs) as efficient computing models has provided an alternative tool for the estimation of PGA by using the actual seismic data without any simplification and assumptions. This paper presents the application of multi-layer perceptron in estimating PGA, and is based on the M.Tech. thesis of the first author (Arjun, 2008).

In the following sections of the paper, the compilation and processing of strong ground motion data for the Japanese earthquake records from Kyoshin-Net database is reviewed and a brief conceptualization of neural networks is presented. In addition, the application of ANN for the estimation of PGA along with the simulation results is presented.

COMPILATION OF STRONG GROUND MOTION DATA

The database used in the study is taken from Kyoshin Net (K-NET) database. Kyoshin Net is a dense strong-motion network consisting of over 1,000 observatories deployed all over Japan at the interval of approximately 25 km. The instruments in these observatories are located on the ground surface. Each station has a digital strong-motion seismograph (i.e., accelerograph) with a wide frequency-band and wide dynamic range. In this study, a total of 84,456 horizontal components of earthquake records from 609 earthquakes of Japan with the magnitude of 5 and above have been downloaded from the internet

(Kyoshin Network[1]). The magnitude scale used by Kyoshin Net is the JMA magnitude M_{JMA} estimated by the Japan Meteorological Agency (JMA). Almost all the sites have the data on soil conditions, e.g., standard penetration value, density, while including the P- and S-wave velocities recorded, except for a few stations where this soil data is not available.

All stations operated by K-NET have K-NET95 accelerometers, with 108 dB dynamic range having a maximum measurable acceleration of 20 m/s^2 (i.e., 2000 Gals). The resolution of A/D converter is 18 bits with a sampling frequency of 100 Hz. The resolution of accelerometer is 1.5 m/s^2. For processing the strong-motion data, a computer program developed by the second author has been used. In this program, the raw data available in terms of counts in the data format of K-NET has been converted into acceleration values by using the scale factor given in the header of data. As the natural frequencies of all accelerographs were very high (i.e., about 200 Hz), there was no need of the instrument response correction.

A baseline correction of all acceleration time histories has been performed by using the least square line of the time history. Corrections have also been applied in frequency domain by filtering the high- and low-frequency components of the accelerograms. All accelerograms were bandpass filtered by removing the frequencies below 0.1 Hz and above 30 Hz. A sixth-order Butterworth bandpass filter was used for this filtering operation.

All the 84,456 horizontal components of the earthquake records were manually viewed by plotting the acceleration time histories, and it was observed that in some of the time histories, two or more events had taken place. All such records with multiple events have been considered only up to the end of the first event by changing the duration of the motion in the header of the data format.

The average values of shear wave velocity, primary wave velocity, standard penetration test (SPT) blow count, and the density of soil have been used. The averaging of these parameters has been done as per FEMA-356 (FEMA, 2000). These values were calculated as shown below:

$$\bar{v}_s, \bar{v}_p, \bar{N}, \bar{\rho} = \frac{\sum_{i=1}^{n} d_i}{\sum_{i=1}^{n} \frac{d_i}{v_{si}}, \frac{d_i}{v_{pi}}, \frac{d_i}{N_i}, \frac{d_i}{\rho_i}} \tag{1}$$

where v_{si} denotes the shear wave velocity of soil, v_{pi} the primary wave velocity of soil, N_i the SPT blow count, and ρ_i the density of soil, in the layer *i*; d_i denotes the depth of the layer *i*; and n denotes the number of layers of the similar soil materials for which data is available.

ARTIFICIAL NEURAL NETWORKS

Artificial neural networks are among the most powerful learning models that are capable of establishing a mapping relationship between the given sets of inputs and outputs. The theoretical background on neural networks (NN) can be found in a large volume of literature (e.g., Zurada, 1992; Hagan et al., 1996; Bishop, 1995; Mehrotra et al., 1996; Haykin, 1994; Demuth et al., 2006). Here, only a brief conceptualization of neural networks is given.

There is no universally accepted definition of an artificial neural network. It is a massively parallel-distributed information processing system that has certain performance characteristics resembling the biological neural networks of the human brain (Haykin, 1994).

Neural networks have been inspired by the neuronal architecture of the brain. A neuron is the information-processing unit of the neural network, much like the brain in human beings (Haykin, 1994). Figure 1 shows the block diagram of a neuron.

A neuron consists of three main parts: a set of synapses, which connect the input signal x_j to the neuron via a set of weights, w_{kj}; an adder u_k which sums up the input signals, weighted by the respective

[1] Website of Kyoshin Network, http://www.k-net.bosai.go.jp

synapses of the neuron; and an activation function $\phi(.)$ for limiting the amplitude of the output of the neuron. At times, a bias b_k is added to the neuron to increase or decrease the net output of the neuron.

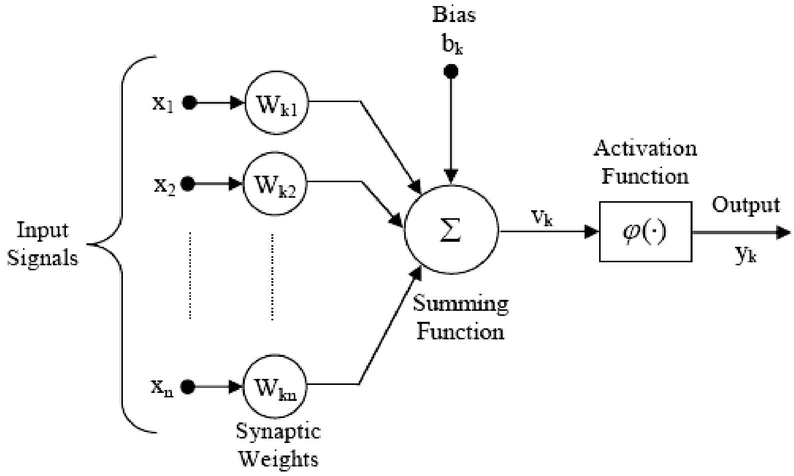

Fig. 1 The block diagram of a neuron (Haykin, 1994)

Mathematically, a neuron k is described as (Haykin, 1994)

$$u_k = \sum_{j=1}^{n} w_{kj} x_j \tag{2}$$

$$y_k = \phi(u_k + b_k) \tag{3}$$

where $x_1, x_2, x_3, \ldots, x_n$ are the input signals; $w_{k1}, w_{k2}, \ldots, w_{kn}$ are the weights for the neuron k; b_k is the bias; u_k is the adder or the linear combiner; $\phi(.)$ is the activation function; and y_k is the output signal of the neuron.

The output range of the neuron depends on the type of activation function used. There are four types of activation functions, which are in common use (Demuth et al., 2006), namely, the hard-limit activation function, the log-sigmoid activation function, the tan-sigmoid activation function, and the linear activation function.

1. Multilayer Perceptron

Network architecture refers to the manner in which the neurons are structured and connected to each other. There are a wide variety of networks depending on the nature of the information processing carried out at the individual neurons, the topology of the links, and the algorithm for the adaptation of link weights. Network architectures can generally be classified as (1) single-layer feedforward, (2) multi-layer feedforward, (3) recurrent, and (4) lattice structure (Haykin, 1994). Furthermore, the networks can be fully or partially connected, meaning that neurons in a given layer might not be connected to all the neurons in the preceding or the following layers.

In this study, multi-layer feedforward neural networks, commonly referred to as multilayer perceptrons (MLPs), have been used. Multilayer perceptrons have been applied successfully to solve some of the difficult and diverse problems in several domains including the structural engineering applications. It has a layered architecture consisting of input, hidden, and output layers. The input signal propagates through the network in a forward direction on a layer-by-layer basis. The output of each layer is transmitted to the input of neurons in the next layer through weighted links. The hidden layer aids in performing useful complex computations by extracting progressively more meaningful features from the input layer. Figure 2 shows a one-hidden-layer MLP with *D* inputs, *K* hidden processing elements and *M* outputs (i.e., MLP (*D-K-M*)).

Training and weight adaptation is done in MLPs in a supervised manner with a highly popular algorithm known as the error back-propagation algorithm. Back-propagation is a very powerful and computationally efficient algorithm. Back-propagation learning consists of two phases. During the first phase, inputs presented to the input layer propagate through the network, layer by layer, to the output layer, where the error between the desired output and the network output is calculated. During this phase, the weights are not modified, and they remain constant. During the second phase, the error signal is propagated backwards from the output layer through the network to the input layer. During this stage, the weights are adjusted in such a way that the actual output moves closer to the desired output. The following equation is used for the adjustment of connection weights:

$$\Delta w_{ij}(n) = \eta(\partial E / \partial w_{ij}) + \alpha \Delta w_{ij}(n-1) j \tag{4}$$

where $\Delta w_{ij}(n)$ and $\Delta w_{ij}(n-1)$ are the weight increments between the nodes i and j during the nth and $(n-1)$th epoch; η is the learning rate; and α is the momentum.

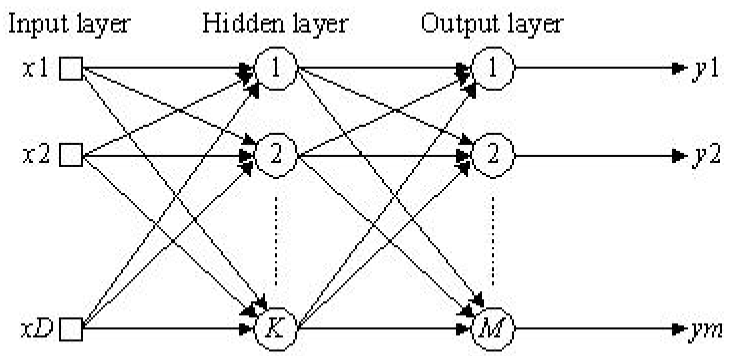

Fig. 2 Multilayer perceptron, MLP (*D-K-M*), with one hidden layer

The momentum factor can speed up training in the very flat regions of the error surface and help prevent oscillations in the weights. A learning rate is used to increase the chance of avoiding the training process being trapped in the local minima instead of global minima. The derivation of the back-propagation algorithm can be found in the literature (Haykin, 1994).

2. Implementation of Back-Propagation Algorithm

Networks have been trained in this study by using the gradient descent with momentum learning scheme, which focuses on using the error between the network output and the desired output. The learning algorithm adapts the weights of the system based on the error until the system produces the desired output. The software NeuroSolutions, version 5.0 (NeuroDimension, Inc.[2]) was used for the simulation of neural network models. The 'Error Criteria' family in NeuroSolutions computes different error measures that can be used to train the network. In this study, the criterion used is the L_2-norm or mean squared error (MSE) criterion. It simply computes the difference between the system output and the desired signal and squares it.

The stopping criteria should be such that it addresses the problem of generalization. This has been done by stopping the training at the point of maximum generalization. The training set is usually divided into two sets: the training and the cross-validation sets. The training is stopped when the error in the cross-validation set is smallest. This will be the point of maximum generalization.

APPLICATION OF ANN FOR ESTIMATING PGA

In this study, the earthquake records from Kyoshin Net database have been used for training the neural networks. A total of 1,850 horizontal components of earthquake records from the 145 earthquakes of magnitudes more than 5.0, and with hypocentral distances of less than 50 km, have been used for training the networks. Figure 3 gives the scatter plot of magnitude versus hypocentral distance of the data used.

An average of the two horizontal components has been used for the computation of peak ground acceleration. The so-obtained set of 925 values from the 145 earthquakes has been used for training and testing the neural networks.

[2] Website of NeuroDimension, Inc., http://www.nd.com

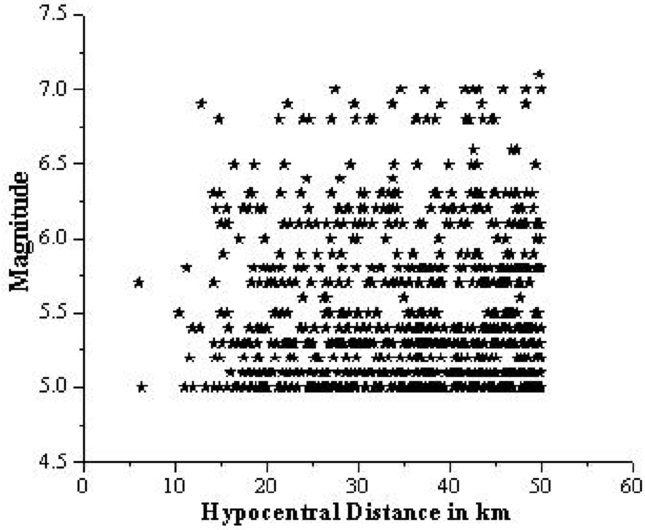

Fig. 3 Scatter plot of magnitude versus hypocentral distance

The prediction of PGA using ANN has been taken up in two stages. In the first stage, earthquake magnitude M, hypocentral distance H, average SPT blow count $\bar{N}$, average primary wave velocity $\bar{v}_p$, average shear wave velocity $\bar{v}_s$, and average density $\bar{\rho}$ of soil have been used as the input variables, and peak ground acceleration has been considered as the output variable. In the second stage, the neural network with three nodes on the input layer representing earthquake magnitude M, hypocentral distance H, and the average shear wave velocity $\bar{v}_s$ has been created, and PGA has been considered as the output. The database has the values of H ranging from 0 to 50 km, $\bar{N}$ ranging from 1 to 99, $\bar{v}_p$ ranging from 450 to 3590 m/s, $\bar{v}_s$ ranging from 85 to 1676 m/s and $\bar{\rho}$ ranging from 1125 to 2425 kg/m^3.

The total set of 925 values has been divided into three sets:

1. training set,
2. validation set, and
3. testing set.

The training set, which is about 80% of the complete dataset, has been used to train the network; the validation set, which is about 10%, has been used for the purpose of monitoring the training process, and to guard against overtraining; and the testing set, which is about 10%, has been used to judge the performance of the trained network. The training was stopped when the cross-validation error began to increase, i.e., when the cross-validation error was minimum.

1. Six Inputs-Based Network

The ANN model with six nodes on the input layer has been created. The six nodes represent the earthquake magnitude M, hypocentral distance H, average SPT blow count $\bar{N}$, average primary wave velocity $\bar{v}_p$, average shear wave velocity $\bar{v}_s$, and average density $\bar{\rho}$ of soil. A set of 825 values was selected randomly from the total set of 925 values for training and cross-validation, and the remaining set of 100 values was used to test the performance of the trained networks. Four different datasets of 825 values were created and randomized. The four datasets were trained independently, and the dataset, which gave the minimum mean square error (MSE), was considered for testing the network. Parametric studies have been carried out in order to evaluate the optimum values of the hidden nodes and learning parameters. Various parameters used for training the network are given in Table 1. Figure 4 shows one hidden layer network model, with 15 hidden neurons, six input neurons and one output neuron.

Typical trained patterns have been presented in Table 2 for the six inputs-based network. In this table, MSET represents the mean square error of the training set, and MSECV represents the mean square error of the validation set. The network with 15 hidden neurons in the hidden layer (i.e., 6-15-1) showed the best performance with minimum MSE.

Table 1: Parameters for Neural Network with One Hidden Layer for Six Inputs

Description	Hidden Layer	Output Layer
Transfer Function	TanhAxon	SigmoidAxon
Learning Rule	Momentum	Momentum
Step Size	1.0	0.1
Momentum	0.9	0.9

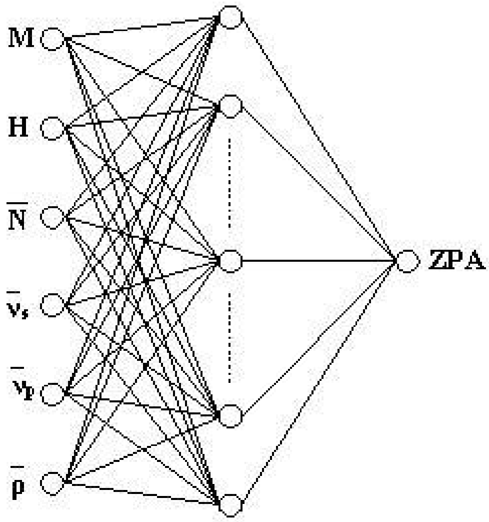

Fig. 4 Neural network architecture with six inputs for the prediction of PGA

Table 2: MSE of Six Inputs-Based Network

Dataset	Network	Epochs	MSET	MSECV	Time Taken (h:min:s)
Dataset 3	6-10-1	10000	1.36×10^{-3}	1.43×10^{-3}	0:02:00
	6-7-1	10000	1.42×10^{-3}	1.50×10^{-3}	0:01:57
	6-14-1	10000	1.35×10^{-3}	1.45×10^{-3}	0:02:25
	6-15-1	10000	1.31×10^{-3}	1.40×10^{-3}	0:02:28
	6-16-1	10000	1.36×10^{-3}	1.44×10^{-3}	0:02:32
	6-18-1	10000	1.34×10^{-3}	1.49×10^{-3}	0:02:39
	6-19-1	10000	1.35×10^{-3}	1.45×10^{-3}	0:02:41
	6-10-1	20000	1.17×10^{-3}	1.32×10^{-3}	0:04:03
	6-18-1	20000	1.16×10^{-3}	1.28×10^{-3}	0:05:41
	6-15-1	20000	1.14×10^{-3}	1.28×10^{-3}	0:05:16
	6-15-1	30000	1.11×10^{-3}	1.19×10^{-3}	0:08:11
	6-15-1	50000	9.33×10^{-4}	1.12×10^{-3}	0:13:50

2. Observations of Six Inputs-Based Network

The results obtained after testing the six inputs-based network were quite promising. These results have been compared by calculating the percentage error between the actual and predicted values of peak ground acceleration. The efficiency of results obtained from the tested network has been categorized as follows:

1. the results with percentage error less than 3% as accurate,
2. the results with percentage error in the range of 3–5% as substantially accurate,
3. the results with percentage error in the range of 5–10% as moderately accurate, and
4. the results with percentage error more than 10% as incorrect.

The efficiency of results, which have been categorized as above, is tabulated in Table 3. The comparison between the desired PGA and the ANN output with six inputs is shown in Figure 5.

Table 3: Efficiency of the Six Inputs-Based Network

Serial No.	Efficiency	Percentage
1	Accurate	65
2	Substantially Accurate	10
3	Moderately Accurate	5
4	Incorrect	20

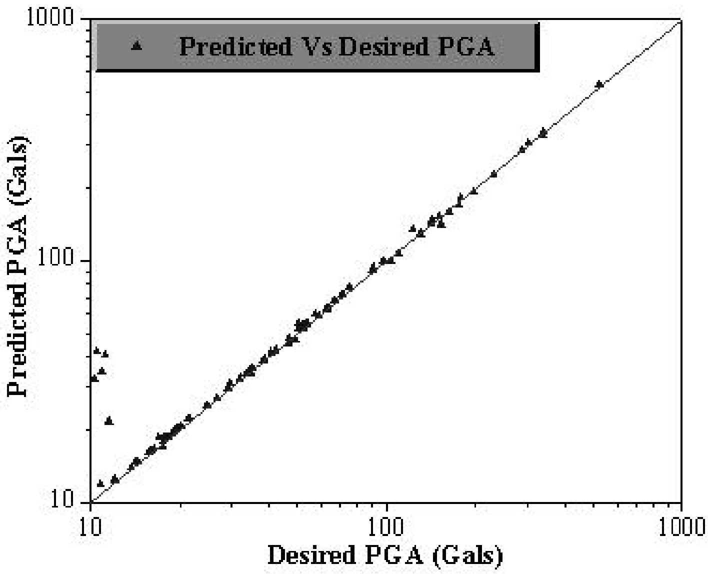

Fig. 5 Scatter plot of predicted PGA versus desired PGA (with six inputs)

From the results, it is seen that the ANN with six inputs has predicted 65% accurate results on PGA along with some inaccurate results. It is also observed that the incorrect results are for the PGAs less than 0.1 m/s^2 (i.e., 10 Gals). It can therefore be concluded that ANN cannot predict lower peak ground accelerations correctly with the above trained network. This could be either due to the reason of overgeneralization during the training or because the training space contained very little data pertaining to the PGA less than 0.1 m/s^2 (i.e., 10 Gals).

3. Three Inputs-Based Network

Except the K-Net strong motion database of Japan, no other database provides the detailed soil condition data at the recording stations. Only few databases provide the average shear wave velocity $\overline{v}_s$ recorded at the stations. Therefore, for the use of trained networks based on the Japanese strong motion data in other countries, it is essential to train the networks for three inputs.

An ANN model with three nodes on the input layer has been created. The three nodes represent the earthquake magnitude M , hypocentral distance H , and average shear wave velocity $\overline{v}_s$. Similar to the six inputs-based network, a set of 825 values was selected randomly from the total set of 925 values for the purpose of training and cross-validation, and the remaining 100 values were used to test the performance of the trained networks. Four different datasets of 825 were created and randomized. The four data sets were trained independently, and the dataset, which gave the minimum mean square error (MSE), was considered for testing the network. The parameters used for training the network are given in Table 4. Figure 6 shows a hidden layer network model, with 18 hidden neurons, three input neurons and one output neuron.

Typical trained patterns have been presented in Table 5 for the three inputs-based network. In this table, MSET represents the mean square error of the training set, and MSECV represents the mean square error of the validation set. The network with 18 hidden neurons in the hidden layer (i.e., 3-18-1) showed the best performance with minimum MSE.

Table 4: Parameters for Neural Network with One Hidden Layer for Three Inputs

Description	Hidden Layer	Output Layer
Transfer Function	TanhAxon	SigmoidAxon
Learning Rule	Momentum	Momentum
Step Size	1.0	0.1
Momentum	0.9	0.9

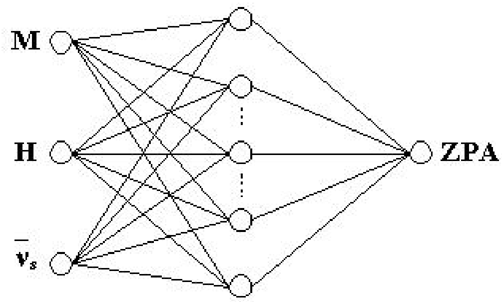

Fig. 6 Neural network architecture with three inputs for the prediction of PGA

Table 5: MSE of Three Inputs-Based Network

Dataset	Network	Epochs	MSET	MSECV	Time Taken (h:min:s)
Dataset 4	3-4-1	10000	1.56×10^{-3}	1.93×10^{-3}	0:01:39
	3-10-1	10000	1.55×10^{-3}	1.85×10^{-3}	0:01:57
	3-15-1	10000	1.49×10^{-3}	1.71×10^{-3}	0:02:18
	3-15-1	20000	1.48×10^{-3}	1.67×10^{-3}	0:05:07
	3-18-1	10000	1.43×10^{-3}	1.62×10^{-3}	0:02:22
	3-18-1	20000	1.41×10^{-3}	1.59×10^{-3}	0:05:49
	3-18-1	30000	1.39×10^{-3}	1.53×10^{-3}	0:07:41
	3-18-1	40000	1.38×10^{-3}	1.52×10^{-3}	0:10:39
	3-18-1	50000	1.37×10^{-3}	1.51×10^{-3}	0:13:10

The efficiency of results obtained from the tested network has been categorized in a similar manner as that of the results from the six inputs-based network. The efficiency of results has been presented in Table 6. Figure 7 shows the scattered plot of desired PGA versus predicted PGA.

4. Observations of Three Inputs-Based Network

From the results presented, it is observed that the percentage of accurate results with three inputs is less when compared with that with six inputs. Further, it is observed that the trained networks are not capable of mapping peak ground accelerations less than about 0.2 m/s^2.

5. Testing of Trained Network for Few Significant U.S. Earthquakes

Only few organizations provide information on the average shear wave velocity $\bar{V}_s$ recorded at the stations. One such organization that provides the average shear wave velocity $\bar{V}_s$ recorded at the stations is the California Strong Motion Instrumentation Program (CSMIP). In this study, the processed data from the CSMIP database has been taken. The data consists of the ground motion recorded at a particular station for a particular event. In addition, for each recording station the average shear wave velocity $\bar{V}_s$, as recorded, is also available. The earthquake magnitude M, the hypocentral distance H, and the average shear wave velocity $\overline{v}_s$ are considered as the inputs, and the PGA is considered as the output. An average of the two horizontal components has been used for the computing the PGA. It has been found by Katsumata (1996) that the average difference between M_{JMA} and moment magnitude M_w is not significant for the earthquakes in the magnitude range from 5 to 7. The networks trained with three inputs for the K-Net records were tested for a few significant CSMIP records. The testing has been done for the following records:

1. Loma Prieta Earthquake record (M_w = 7.0; October 17, 1989; Eureka Canyon Road, Corralitos station),
2. Big Bear Earthquake record (M_w = 6.4; June 28, 1992; Civic Center Grounds, Big Bear Lake station),
3. Northridge Earthquake record (M_w = 6.7; January 17, 1994; Cedar Hill Nursery A, Tarzana station), and
4. Parkfield Earthquake record (M_w = 6.0; September 28, 2004; Gold Hill 3W, Parkfield station).

The PGAs predicted by the neural network (trained for three inputs) for these ground motions are tabulated in Table 7.

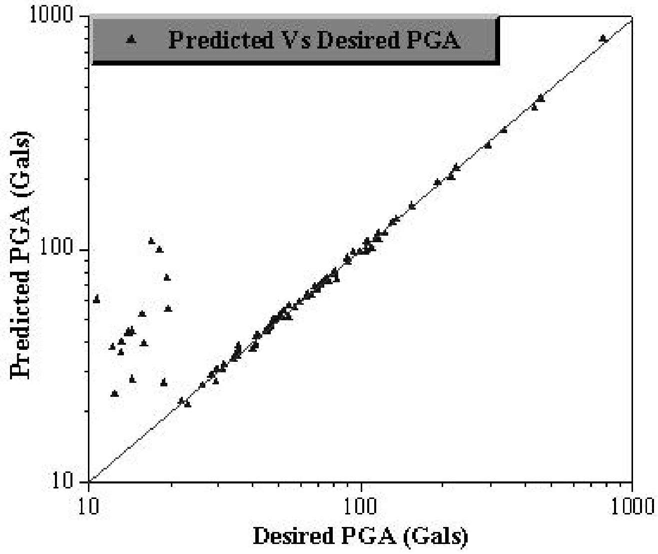

Fig. 7 Scatter plot of predicted PGA versus desired PGA (with three inputs)

Table 6: Efficiency of the Three Inputs-Based Network

Serial No.	Efficiency	Percentage
1	Accurate	44
2	Substantially Accurate	20
3	Moderately Accurate	12
4	Incorrect	24

CONCLUSIONS

A multi-layer perceptron architecture with the error back-propagation learning algorithm has been adopted to estimate peak ground accelerations for the Japanese earthquake records with earthquake magnitudes more than 5.0 and hypocentral distances less than 50 km. The PGAs predicted by the ANN with six inputs have been found to be more accurate in comparison with the three-inputs case. From these observations it has been concluded that the perceptron model is quite promising for the estimation of peak ground acceleration and that the obtained results might be of significant importance for future project sites coming up near the active faults with expected hypocentral distances less than 50 km. The PGAs predicted with six inputs showed accurate results (with percentage errors less than 3%) for 65% cases, whereas, in the case of three inputs, 44% of the predicted PGAs showed accurate results. It has been also seen that a majority of the incorrect results (with percentage errors more than 10%) are for the lower peak ground accelerations. A careful selection of the data may enhance the predictions, especially in the case of PGAs more than 0.1 m/s^2 (i.e., 10 Gals). The PGAs predicted by the three inputs-based network for a few significant U.S. earthquakes were found to be quite close to the desired values and generally on the higher side.

Table 7: PGAs Predicted by the Three Inputs-Based Network

Earthquake	M	H (km)	$\bar{V}_s$ (m/s)	Desired PGA (m/s^2)	Network PGA (m/s^2)	Percentage Error
Loma Prieta	7.0	20.13	462	5.435	5.947	9.42
Big Bear	6.5	12.9	339	5.032	5.284	5.00
Northridge	6.4	18.7	257	13.576	11.786	13.18
Parkfield	6.0	9.5	438	5.372	5.685	5.82
Percentage Error = 100×|(Network PGA–Desired PGA)|/|Desired PGA|						

Results of the predicted PGA have indicated that ANN is a promising tool for the estimation of peak ground acceleration at a site. The performance of networks may be improved by carrying a detailed parametric study on the optimal network to be used for predicting the peak ground acceleration. Future work may also examine the application of hybrid artificial intelligence techniques.

ACKNOWLEDGEMENTS

The authors wish to thank Kyoshin Net Strong Motion Network of Japan for providing an excellent earthquake database for conducting this research. This support is gratefully acknowledged.

REFERENCES

1. Arjun, C.R. (2008). “Application of Artificial Neural Networks for Generating Strong Ground Motion Parameters”, M.Tech. Thesis, Department of Earthquake Engineering, Indian Institute of Technology Roorkee, Roorkee.
2. Bishop, C.M. (1995). “Neural Networks for Pattern Recognition”, Oxford University Press, Oxford, U.K.
3. Demuth, H., Beale, M. and Hagan, M. (2006). “Neural Network Toolbox 5: User’s Guide”, The MathWorks, Inc., Natick, U.S.A.
4. Douglas, J. (2003). “Earthquake Ground Motion Estimation Using Strong-Motion Records: A Review of Equations for the Estimation of Peak Ground Acceleration and Response Spectral Ordinates”, Earth-Science Reviews, Vol. 61, No. 1-2, pp. 43–104.
5. FEMA (2000). “Prestandard and Commentry for the Seismic Rehabilitation of Buildings”, Report FEMA 356, Federal Emergency Management Agency, Washington, DC, U.S.A.
6. Hagan, M.T., Demuth, H.B. and Beale, M. (1996). “Neural Network Design”, PWS Publishing Company, Boston, U.S.A.
7. Haykin, S. (1994). “Neural Networks: A Comprehensive Foundation”, Prentice-Hall, Inc., New Jersey, U.S.A.
8. Katsumata, A. (1996). “Comparison of Magnitudes Estimated by the Japan Meteorological Agency with Moment Magnitudes for Intermediate and Deep Earthquakes”, Bulletin of the Seismological Society of America, Vol. 86, No. 3, pp. 832–842.
9. Mehrotra, K., Mohan, C.K. and Ranka, S. (1996). “Elements of Artificial Neural Networks”, Penram International Publishing (India) Pvt. Ltd., Mumbai.
10. Zurada, J.M. (1992). “Introduction to Artificial Neural Systems”, West Publishing Company, St. Paul, U.S.A.

ISET Journal of Earthquake Technology, Paper No. 502, Vol. 46, No. 1, March 2009, pp. 29–45

SEISMIC PERFORMANCE AND VULNERABILITY OF INDIAN CODE-DESIGNED RC FRAME BUILDINGS

Putul Haldar and Yogendra Singh
Department of Earthquake Engineering
Indian Institute of Technology Roorkee
Roorkee-247667

ABSTRACT

The current seismic design practice in India is based on the force-based design philosophy, with a partial incorporation of the capacity design concepts. In the present study, the adequacy of this philosophy and relative importance of various code provisions are examined by estimating the expected performance of a set of code-designed buildings, in deterministic as well as in probabilistic terms. The FEMA-440 and HAZUS methodologies are used for estimating the seismic performance and vulnerability. It is shown that the Special Moment-Resisting Frame design under the current design provisions of Indian standards has a higher probability of damage, as compared with the Ordinary Moment-Resisting Frame design, because of the higher allowable ultimate drift limit. It is also shown that the deterministic framework of performance-based seismic design does not provide complete insight into the expected performance and associated risks of the designed buildings.

KEYWORDS: Force-Based Design, Pushover Analysis, Seismic Performance, Vulnerability, RC Frame Buildings

INTRODUCTION

Earthquake-resistant design (ERD) of structures has developed greatly since the initial ideas took shape in the early twentieth century. The invention of accelerograph and development of the concept of response spectrum are the most important steps in the history of ERD. The other important development, at the philosophical level, was the understanding of ductility and hysteretic damping. Gradually, the earthquake-resistant design has developed significantly in the form of capacity design, displacement-based design, and performance-based design.

Code design practices have been traditionally based on the force-based design (FBD) concept, in which individual components of the structure are proportioned for strength (such that the structure can sustain the shocks of moderate intensities without structural damage and the shocks of heavy intensities without total collapse) on the basis of internal forces computed from the elastic analysis. The inelastic effects are indirectly accounted for by using a response reduction factor, which is based on some form of the equal-displacement and equal-energy principles. In the code procedures, an explicit assessment of the anticipated performance of the structure is not made. In order to ensure the desired seismic performance, the design codes exercise three types of controls in design:

1. Control of ductility demand, by using the effective response reduction factor I/R, where I represents the importance factor, and R represents the reduction factor for ductility and overstrength. Overstrength arises due to the use of material and load safety factors, and due to the characteristic strength (or grade) of material defined as the 95% confidence value.
2. Control of minimum design base shear, through the use of ‘capping’ on the design natural period and/or ‘flooring’ on the design base shear.
3. Control of flexibility, through the limit of maximum permissible interstorey drift.

The seismic performance of a building, designed according to the code practices, depends on the overall effect of the above controls and several other provisions for the design and detailing, and the role of an individual control parameter is not explicit in ensuring the desired performance.

Another emphasis of the code-based design is the enhancement of ductility by proper detailing and proportioning of members. Ductility can be enhanced by facilitating plastic deformations only in the desirable ductile modes. This can be achieved by designing the brittle modes/members to have strengths higher than the ductile modes. With the desired strength hierarchy incorporated among the structural elements, this concept of "capacity design" introduced by Park and Paulay (1975) has become an integral part of the national design codes.

Priestley (1993, 2000, 2003) and other researchers have pointed out that force is a poor indicator of the damage and that there is no clear relationship between the strength and the damage. Hence, force cannot be a sole criterion for design. Further, assuming a flat value of the response reduction factor for a class of buildings is not realistic, because ductility depends on so many factors, such as degree of redundancy, axial force, steel ratio, structural geometry, etc. To overcome these flaws in the force-based design, an alternative design philosophy named "displacement-based design" was first introduced by Qi and Moehle (1991), which included translational displacement, rotation, strain, etc. in the basic design criteria. This philosophy is a very promising design tool that enables a designer to design a structure with predictable performance. A considerable research effort has been devoted to this area in the past few decades and different variants of this method have been developed, in which different deflection parameters are chosen as the performance indicators and different techniques are used to proportion the members to achieve the desired performance. One of the well-developed approaches for the performance evaluation and rehabilitation of existing buildings has been documented by FEMA-356 (FEMA, 2000) and ASCE-41 (ASCE, 2007). This approach uses the plastic deformations in members as the performance indicators and can be extended to the new buildings as well. However, since no methodology has been presented for the systematic proportioning of structural components to achieve the desired performance in case of new buildings, it may require a large number of iterations. Priestley and his group (Priestley, 2000; Priestley et al., 2007) have made significant contributions in developing a practical methodology for the displacement-based design. In their approach, the interstorey drifts and ductility demand are considered as the control parameters for ensuring the desired performance. They have specified engineering limit states for different performance levels, and a draft code on the displacement-based design has also been proposed (Priestley et al., 2007).

In the present study, adequacy and relative importance of various provisions of the current Indian standard (BIS, 2002), which follows a force-based design methodology similar to many other national codes, has been examined. Expected seismic performance and vulnerability of the 4-storey and 9-storey generic RC frame buildings have been studied by using FEMA-356 (FEMA, 2000) and HAZUS-MH (NIBS, 2003). The roles of different code provisions for overstrength and ductility, control of design base shear, and control of flexibility, in the seismic performance and vulnerability of code-designed buildings have been examined.

KEY PROVISIONS OF INDIAN SEISMIC DESIGN CODES

The Indian code of practice for seismic design, i.e., IS 1893 (BIS, 2002), defines two levels of seismic hazard, namely Maximum Considered Earthquake (MCE) and Design Basis Earthquake (DBE). The effective peak ground acceleration (EPGA) in the case of DBE is considered as half of the EPGA for MCE, and structures are designed for DBE with the use of partial load and material safety factors. The buildings are designed for the base shear calculated as

$$V_B = \frac{Z}{2}\frac{I}{R}\frac{S_a}{g}W \tag{1}$$

where, zone factor Z represents the EPGA; and response reduction factor R and importance factor I control the ductility demand, based on the anticipated ductility capacity and the post-earthquake importance of the structure, respectively.

Based on the reinforcement detailing and capacity design, two ductility classes for RC buildings, Ordinary Moment-Resisting Frame (OMRF) and Special Moment-Resisting Frame (SMRF), are specified. The Indian standard IS 13920 (BIS, 1993) provides the specifications for ductile reinforcement detailing and capacity design in the case of SMRF. In general, the reinforcement detailing and capacity design provisions of the Indian code for OMRF and SMRF correspond to those for OMRF and Intermediate Moment Resistant Frame (IMRF), respectively, in ASCE-7 (ASCE, 2006) and ACI-318 (ACI, 2008). There is no class of RC frames in the Indian code (BIS, 2002) corresponding to SMRF in ASCE-7 and ACI-318. As compared to the Eurocode 8 (BSI, 2004), OMRF and SMRF of Indian code correspond to the ductility classes, 'low' and 'medium', and there is no class defined (in the Indian code) corresponding to the ductility class 'high' of the Eurocode 8. This indicates the inadequacy of ductility provisions in the Indian code (BIS, 1993) as compared to ACI-318 and Eurocode 8. However, the response reduction factors of 3 and 5, specified in the Indian code (BIS, 2002) for OMRF and SMRF, respectively, are much higher than the corresponding values of behaviour factor specified in the Eurocode 8 for the respective ductility classes. Considering that the ductility provisions for OMRF are inadequate, the Indian code (BIS, 2002) prohibits the OMRF design in moderate and high seismic areas; but due to the weak enforcement, this type of construction is prevailing and hence is considered in this study. Interestingly, the Indian code (BIS, 1993) does not ensure the strong column-weak beam design, even in the case of Special Moment-Resisting Frame. Since it is a widely recognized design criterion, the present study has been conducted while ensuring the strong column-weak beam design for SMRF.

In practice, the designers have a tendency to make flexible buildings, as this results in a lower design base shear due to a longer period of vibration. To safeguard against this error, the code (BIS, 2002) has recommended a capping on the natural period used for the base shear calculation. Empirical expressions for the design natural periods for different type of buildings have been provided in the code, e.g., the expression for the RC frame buildings is

$$T_a = 0.075h^{0.75} \tag{2}$$

where T_a (in s) is the design natural period of a building having the height equal to h (in m). The capping is implemented by scaling all the response quantities by a factor equal to $\overline{V}_B / V_B$, where $\overline{V}_B$ is the base shear calculated by using the empirical design period and V_B is the base shear obtained by using the time period estimated analytically.

Contrary to many other national codes, the Indian standard (BIS, 2002) specifies a limit of 0.4% for the interstorey drifts at the design (or elastic) force level, while in the IBC (ICC, 2006) and Eurocode 8 (BSI, 2004), limits are specified for the total interstorey drift (including the elastic and inelastic components). As different reduction factors (and hence, different ductility demands) have been specified for Ordinary Moment-Resisting Frames and Special Moment-Resisting Frames, this results in different limits on the total drift. Considering the equal-displacement principle to be valid, the design drift limit as per the Indian standard leads to the values of 1.2% and 2.0% for the total interstorey drift for Ordinary Moment-Resisting Frames and Special Moment-Resisting Frames, respectively. This is not only considerably higher than the limits specified in the Eurocode 8, this also means that SMRF can be designed for about a 1.67 times higher interstorey drift, as compared to OMRF. Further, the Indian standard does not specify any additional control over the plastic deformations in structural and non-structural components as in the Eurocode 8.

In addition to the above provisions, the design of RC buildings is governed by the general design provisions of the Indian standard IS 456 (BIS, 2000). The provisions in this code most relevant to the present study are on the control of beam deflections for the serviceability limit state and on the minimum reinforcement requirements. These criteria govern the member sizes and reinforcement quantity in some cases, thus contributing to overstrength, and have also been considered in the present study.

PARAMETRIC STUDY

A parametric study has been carried out on a set of multistorey RC frame buildings to assess the efficacy of the different provisions of the Indian standards (BIS, 456, 1993, 2002) and to study the effects of different design considerations on the anticipated seismic performance and vulnerability of buildings.

1. Design of Generic Buildings

The RC buildings, as considered in the parametric study, have an identical plan geometry, as shown in Figure 1, and have two heights—4 storeys and 9 storeys. The plan considered here is of an existing hospital building in New Delhi. It is symmetric in the transverse direction and slightly asymmetric in the longitudinal direction, and has significantly different redundancies in the two directions. Further, the spans of the beams in the two directions are also quite different, representing the characteristics of a wide range of real buildings. The storey height has been considered as 3.3 m, with the foundations being 1.5 m below the ground level. The corridor is free from the transverse beams, which is a typical feature of the commercial and institutional buildings in India. The buildings have been assumed to be situated on the hard soil in the seismic zone IV (with EPGA = 0.24*g* for MCE). For the design, M20 concrete and Fe415 steel have been used, and member sections have been proportioned to have about 2–4% steel in the columns and about 1% steel (on each face) in the beams, wherever permitted by the other code requirements. The slab thickness has been assumed as 150 mm, and a uniform weight of 0.5 kN/m^2 has been considered due to the partitions.

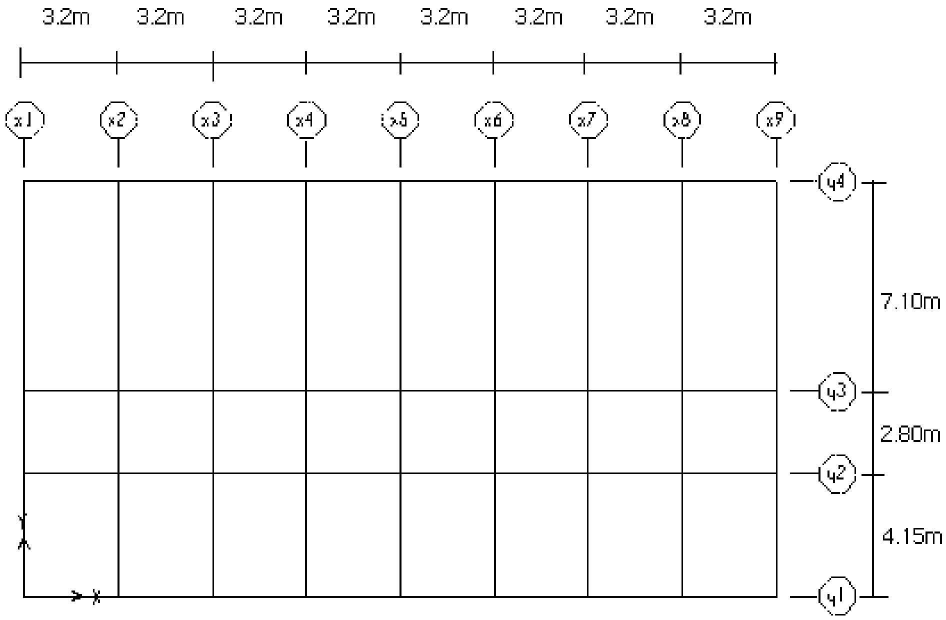

Fig. 1 Plan of buildings

The dead load (DL) and live load (LL) have been calculated by using the Indian standard IS 875, Part 1 (BIS, 1987a) and Part 2 (BIS, 1987b), respectively**.** The seismic design has been performed as per the Indian standard IS 1893 (BIS, 2002), while considering the specified load combinations. Five design levels have been considered for this study. At the 'gravity design' level, the buildings have been designed only for the gravity loads, and no consideration has been given for the seismic forces. Due to the weak enforcement, this type of construction practice is still prevailing in many cases. Further, although not permitted by the Indian standard (BIS, 2002) in the seismic zones III, IV and V, the most common type of construction practice followed in India is that of Ordinary Moment-Resisting Frame, which has been considered with and without period capping in the present study. Similarly, Special Moment-Resisting Frame has also been considered with and without period capping. Preliminary sizes of the beams have been calculated based on the deflection criterion given in the Indian standard IS 456 (BIS, 2000). The minimum and maximum reinforcement criteria of IS 456 and IS 13920 have also been satisfied. For the purpose of comparison, buildings with and without satisfying the maximum drift limit as per the Indian standard IS 1893 have been considered. To study the effect of unequal inelastic drift limits in the cases of Ordinary Moment-Resisting Frame and Special Moment-Resisting Frame, a special case of Special Moment-Resisting Frame, with the inelastic drift limit equalized to that of Ordinary Moment-Resisting Frame, has also been considered.

2. Nonlinear Analysis and Seismic Performance

Nonlinear space frame models of the designed buildings have been developed in the SAP2000 Nonlinear software (CSI, 2006). Lumped plasticity models with the hinge properties, as defined in FEMA-356 (FEMA, 2000), have been used. Conforming 'C' and non-conforming 'NC' transverse reinforcements have been considered for Special Moment-Resisting Frames and Ordinary Moment-Resisting Frames, respectively, to assign the plastic rotations for the beams and columns. In the present study, only the flexural inelastic mechanisms have been considered, assuming that the other failure mechanisms due to shear, bond slip and anchorage have been avoided in the code-based design. However, it is to be noted that these mechanisms may govern the seismic performance of buildings in some cases of gravity-designed and Ordinary Moment-Resisting Frame buildings. Estimating effective stiffness of the cracked RC members is another crucial issue in a nonlinear analysis. Priestley (2003) has pointed out the dependence of effective stiffness on the yield strength of RC members. However, considering this fact in the analysis makes the design process cumbersome and iterative. Therefore, in the present study, the guidelines of FEMA-356 (FEMA, 2000) proposed for the effective stiffness of RC beams and columns have been used for simplicity.

Nonlinear static (pushover) analysis has been carried out to estimate the strength, ductility and expected performance of the designed buildings. The accuracy of pushover analysis depends on a number of factors, including the distribution of lateral load, consideration of higher-mode effects (Chopra and Goel, 2002), and the procedure used to obtain the performance point. In the present study, the parabolic distribution of lateral load, as prescribed by the Indian standard IS 1893 for the distribution of design base shear along the height of the building, has been considered for the pushover analysis, and the Displacement Modification Method of FEMA-440 (FEMA, 2005) has been used for estimating the performance point.

As mentioned earlier, the code method of design considers the effect of hysteretic damping indirectly in the form of response reduction factor R. Actually, R as specified in the codes represents the combined effect of ductility and overstrength. The relative role of these two parameters can be understood with reference to Figure 2. It shows the capacity (or pushover) curve obtained from the nonlinear static analysis of the building, as converted to the ADRS format (i.e., capacity spectrum) and idealized as a bilinear curve. A capacity spectrum can be characterized by two control points: yield point and the ultimate point. The design spectral acceleration S_{ad} represents the nominal (or design) strength required by the seismic code. The structure is designed for this nominal strength along with the partial factors of safety on load combinations and nominal material strengths. This results in overstrength, and the structure yields at a much higher base shear, which is represented by the yield spectral acceleration S_{ay}. In a bilinear representation, the yield point corresponds to the lateral action, at which a sizeable number of members yield and beyond which the response of the structure becomes highly nonlinear. The ultimate point (S_{du}, S_{au}) represents the ultimate strength and deformation capacity of the structure. The elastic design strength S_{ae} corresponds to the hypothetical structure, which is designed to remain elastic during the earthquake, while having the same period as that of the real structure. It is given by the (generally 5%-damping) elastic design response spectrum.

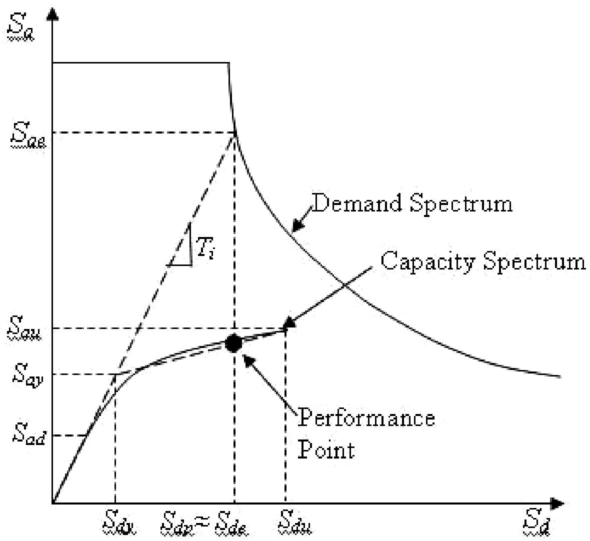

Fig. 2 Demand and capacity curves of a typical structure represented in the acceleration-displacement response spectrum (ADRS) format

The performance point, representing the expected peak displacement of the structure, is the point of intersection of the capacity spectrum with the demand spectrum, which is duly reduced (not shown in Figure 2) for the effect of hysteretic damping exhibited by the structure at the performance point. The equal-displacement principle suggests that displacement at the performance point will be approximately equal to the elastic displacement. Overstrength can be defined in two ways: (i) yield overstrength γ is defined as the ratio of yield spectral acceleration to the design spectral acceleration, S_{ay}/S_{ad}, and (ii) ultimate overstrength λ gives the ratio of ultimate spectral acceleration to the design spectral acceleration S_{au}/S_{ad}. Ductility demand S_{dp}/S_{dy} relates the performance displacement to the yield displacement, and ductility capacity S_{du}/S_{dy} is the available ductility in the structure. Now, the response reduction factor, as per the code (BIS, 2002), can be defined as

$$R = \frac{S_{ae}}{S_{ad}} = \frac{S_{ae}}{S_{ay}} \cdot \frac{S_{ay}}{S_{ad}} = R_{\text{eff}} \cdot \gamma \tag{3}$$

where R_{eff} is the effective reduction factor, representing the ratio of the elastic demand strength to the yield strength. This governs the ductility demand on the structure. According to the equal-displacement principle, the ductility demand μ is approximately equal to R_{eff} for the 'long-period' structures, while for the 'short-period' structures, it is governed by the equal energy principle and is approximately equal to $(R_{\text{eff}}^2 + 1)/2$.

Figures 3 and 4 compare the seismic performances of the 4- and 9-storey gravity-designed buildings with those of the Special Moment-Resisting Frame buildings designed for the seismic zone IV. It can be observed that the earthquake-resistant design and detailing, as per the Indian standards IS 1893 (BIS, 2002) and IS 13920 (BIS, 1993), increases the strength and ductility capacity of the building significantly. However, the relative increase depends strongly on the building height, design period of vibration, and on the span of the beams in the direction under consideration. While in the transverse direction (having a longer span of beams) of the 4-storey building the increase in capacity is about 20%, in the longitudinal direction of the 9-storey building it is about 300%. The figures also show the performance levels (i.e., immediate occupancy (IO), life safety (LS) and collapse prevention (CP) levels) and performance points of the corresponding buildings. The performance levels have been obtained according to the acceptance criteria of FEMA-356 (FEMA, 2000), and performance points have been obtained by using the Displacement Modification Method (DMM) of FEMA-440 (FEMA, 2005). It is to be noted that FEMA-356 specifies the performance limits in terms of the plastic rotations in individual members. The performance levels on the building pushover curve have been marked by identifying the pushover step, at which first member in the building undergoes the plastic rotation (as specified in FEMA-356 for the respective performance limit), and by noting the roof displacement corresponding to that step. With a sufficiently large number of analysis steps, the performance levels can be marked with an acceptable accuracy. It is also interesting to note that in the seismic zone IV, the building designed without any consideration for the earthquake forces satisfies the collapse prevention performance level, even for MCE (except for the 9-storey building, with earthquake ground motion in the longitudinal direction). This means that even if the building is designed and constructed properly for the gravity loads alone, as per the relevant Indian standards (BIS, 1987a, 1987b, 2000), it has sufficient overstrength and ductility to survive, without collapse, the DBE (and in most of the cases, even MCE) level of ground shaking specified by the Indian standard IS 1893 (BIS, 2002) for the seismic zone IV.

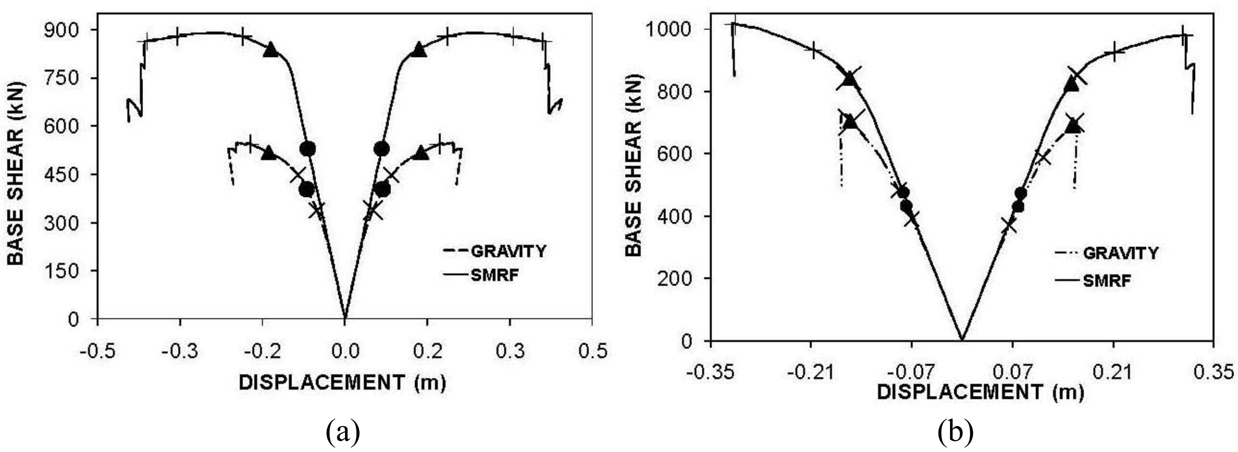

Fig. 3 Comparison of capacity curves and performance points for the 4-storey building designed for gravity and as SMRF, as per the relevant Indian standard (the dot (●) represents the performance point for DBE, and triangle (▲) represents the performance point for MCE; the three crosses (+) represent the IO, LS, and CP performance levels, consecutively): (a) longitudinal direction; (b) transverse direction

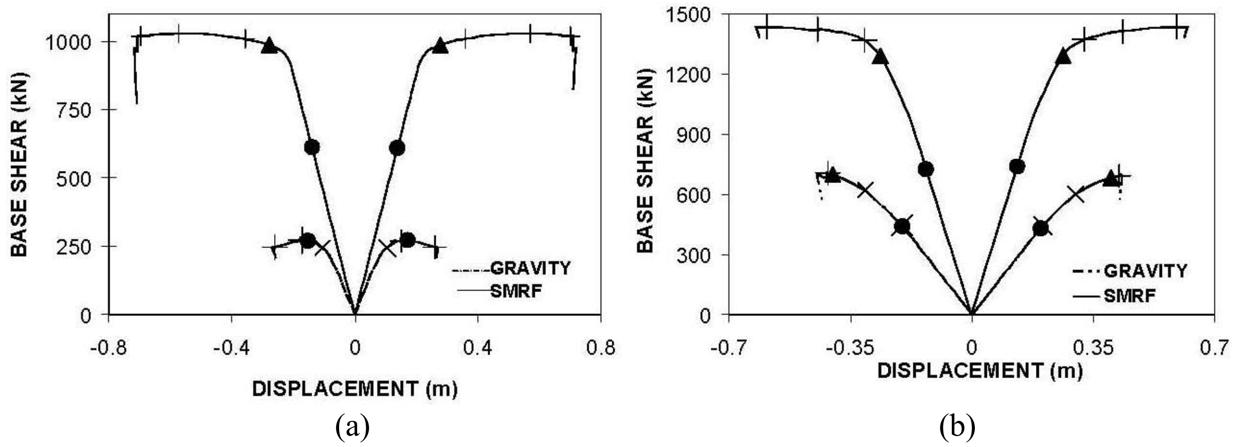

Fig. 4 Comparison of capacity curves and performance points for the 9-storey building designed for gravity and as SMRF, as per the relevant Indian standard (the dot (●) represents the performance point for DBE, and triangle (▲) represents the performance point for MCE; the three crosses (+) represent the IO, LS, and CP performance levels, consecutively): (a) longitudinal direction; (b) transverse direction

Figures 5 and 6 show the relative performances of the 4-storey and 9-storey buildings, respectively, designed as OMRF and SMRF. OMRF represents a lower ductility class of design, and accordingly it is designed for a higher strength. It can be observed that in both cases, the performance level is that of immediate occupancy (i.e., plastic rotations in all the members at the performance point are smaller than those specified by FEMA-356 for the immediate occupancy level) for DBE as well as for MCE. In terms of drift, the performance of OMRF is marginally better, as larger member sections are required in this case.

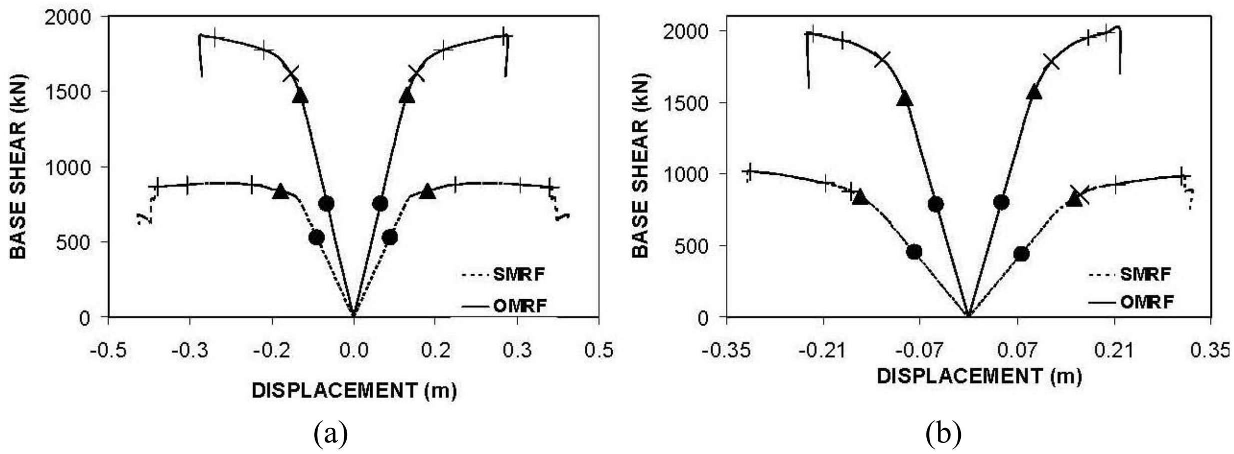

Fig. 5 Comparison of capacity curves and performance points for the 4-storey building designed as SMRF and OMRF, as per the relevant Indian standard (the dot (●) represents the performance point for DBE, and triangle (▲) represents the performance point for MCE; the three crosses (+) represent the IO, LS, and CP performance levels, consecutively): (a) longitudinal direction; (b) transverse direction

The effect of capping on the design periods of buildings, as per the Indian standard IS 1893 (BIS, 2002), has been shown in Figures 7 and 8 for the 4-storey and 9-storey buildings, respectively. The empirical formula recommended in the code (see Equation (2)) results in much smaller periods, as compared to those obtained from the analytical models of the buildings. The natural periods obtained from the analytical models vary from 1.74 to 3.76 s for different designs, while the empirical formula predicts natural periods equal to 0.56 and 0.99 s for the 4-storey and 9-storey buildings, respectively. All these periods are in the velocity-controlled range of the Indian standard design response spectrum (BIS, 2002), resulting in the design base shear inversely proportional to natural period. Accordingly, the capping on design natural period increases the design strength (and hence the yield strength) by a factor of more than 2 in most of the cases. This highlights the importance of capping on the design period in controlling the seismic performance of code-designed buildings. This is clearly demonstrated by Figures 7 and 8, where the buildings designed without capping on period are at the verge of collapse under Maximum Considered Earthquake; while those designed with capping on period have the immediate occupancy performance level, even at Maximum Considered Earthquake. In the case of 4-storey building, it was possible to design for the increased base shear without changing the size of the members, but in the case of 9-storey building, the sizes were also required to be increased. Accordingly, initial stiffness in the case of 4-storey building is same for the capped and uncapped design periods, while in the case of 9-storey building, the initial stiffness for capped period is higher than that for the uncapped period.

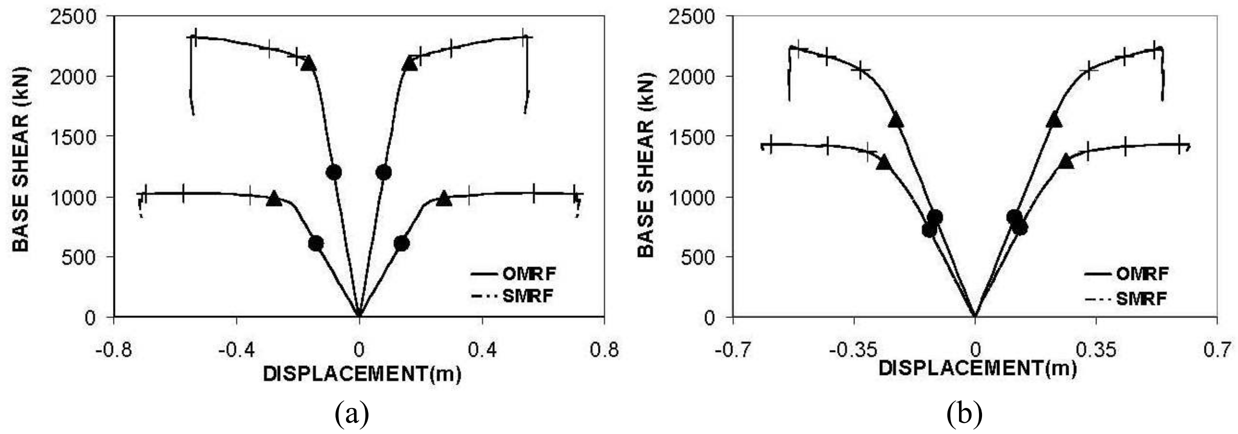

Fig. 6 Comparison of capacity curves and performance points for the 9-storey building designed as SMRF and OMRF, as per the relevant Indian standard (the dot (●) represents the performance point for DBE, and triangle (▲) represents the performance point for MCE; the three crosses (+) represent the IO, LS, and CP performance levels, consecutively): (a) longitudinal direction; (b) transverse direction

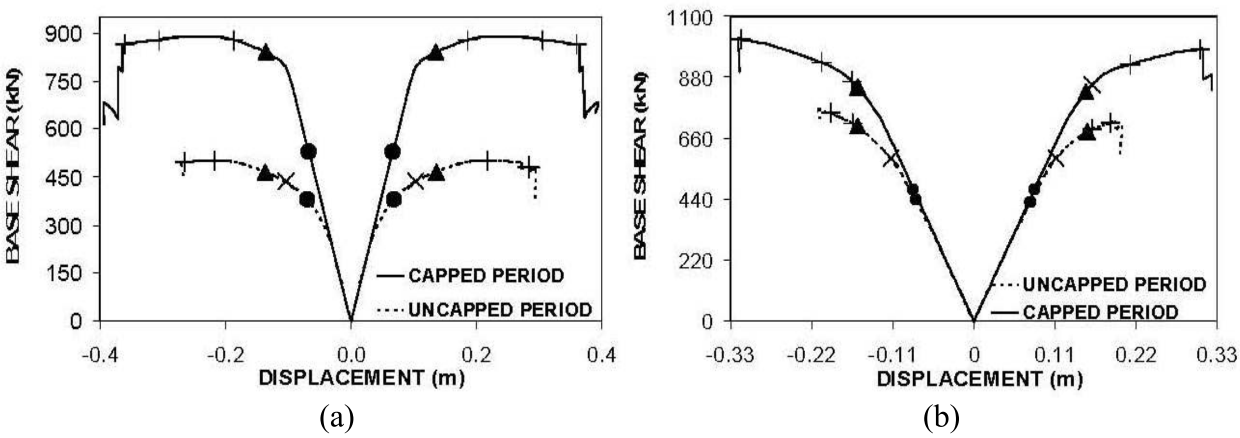

Fig. 7 Comparison of capacity curves and performance points showing the effect of period capping for the 4-storey building designed as SMRF, as per the relevant Indian standard (the dot (●) represents the performance point for DBE, and triangle (▲) represents the performance point for MCE; the three crosses (+) represent the IO, LS, and CP performance levels, consecutively): (a) longitudinal direction; (b) transverse direction

Another interesting observation about the capping on design period, which leads to a discrepancy with respect to the Indian standard provision for the control of drift, can be made from Tables 1 and 2, comparing the bilinear capacity curve and capacity spectrum parameters for all the buildings under investigation. The tables show that the drift control is a governing criterion, only in the case when capping on the design period is applied; although the buildings are stiffer in this case. Further, interstorey drift controls the design in the case of Ordinary Moment-Resisting Frame, while in the case of Special Moment-Resisting Frame it is generally not a governing criterion, even though the Special Moment-Resisting Frame buildings are more flexible than the Ordinary Moment-Resisting Frame buildings. This is because the Indian standard (BIS, 2002) limits the drift at design load (i.e., the elastic drift at reduced load), and not the total drift. This has serious implications towards the performance and vulnerability of the buildings designed as per the code. Further discussion on this aspect is presented in the next section.

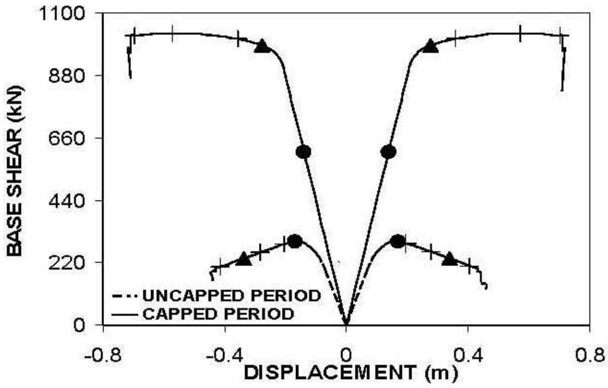

(a)

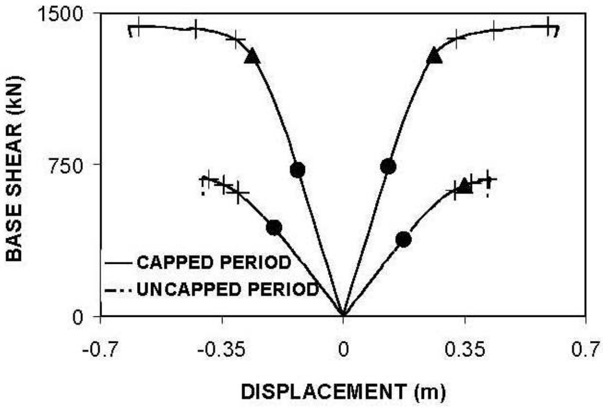

(b)

Fig. 8 Comparison of capacity curves and performance points showing the effect of period capping for the 9-storey building designed as SMRF, as per the relevant Indian standard (the dot (●) represents the performance point for DBE, and triangle (▲) represents the performance point for MCE; the three crosses (+) represent the IO, LS, and CP performance levels, consecutively): (a) longitudinal direction; (b) transverse direction

Table 1: Capacity Curve and Capacity Spectrum Parameters for the 4-Storey Buildings

Direction	Design Level	Interstorey Drift at Design Load	Capacity Curve				Capacity Spectrum			
			Yield Point		Ultimate Point		Yield Point		Ultimate Point	
		D_d/H_{tot} (%)	D_y/H_{tot}	V_y/W	D_u/H_{tot}	V_u/W	S_{dy} (mm)	S_{ay} (g)	S_{du} (mm)	S_{au} (g)
Longitudinal	Gravity-Designed	-	0.004	0.044	0.014	0.057	47	0.051	176	0.066
	OMRF, Uncapped Period	0.15	0.004	0.050	0.017	0.057	51	0.058	203	0.066
	OMRF, Capped Period	0.51	0.012	0.139	0.024	0.150	141	0.160	294	0.173
	OMRF, Capped Period (Drift-Controlled)	0.32	0.007	0.153	0.020	0.168	94	0.179	252	0.197
	SMRF, Uncapped Period	0.09	0.004	0.044	0.020	0.052	47	0.051	246	0.060
	SMRF, Capped Period	0.31	0.008	0.091	0.027	0.093	93	0.105	328	0.107
Transverse	Gravity-Designed	-	0.006	0.054	0.011	0.073	76	0.062	133	0.084
	OMRF, Uncapped Period	0.17	0.006	0.053	0.012	0.076	77	0.062	142	0.087
	OMRF, Capped Period	0.67	0.015	0.133	0.022	0.141	186	0.15	268	0.16
	OMRF, Capped Period (Drift-Controlled)	0.34	0.007	0.160	0.015	0.180	90	0.187	187	0.211
	SMRF, Uncapped Period	0.10	0.007	0.063	0.014	0.080	88	0.072	176	0.092
	SMRF, Capped Period	0.40	0.011	0.091	0.022	0.106	130	0.105	266	0.122

Tables 3 and 4 present the overstrength and ductility parameters for the code-designed buildings. The ductility demand shown in these tables is for MCE. It is observed that the yield overstrength in the Ordinary Moment Resisting Frame buildings as well as in the Special Moment Resisting Frame buildings, which have been designed with period capping and drift control, is of the order of 2. In the case of the buildings designed without period capping, this can be much higher, because the member sizes and reinforcement are governed by the other criteria of the codes. It is interesting to note that the ductility capacity as well as ductility demand are higher in the case of drift-controlled (i.e., stiffer) buildings, as compared to the buildings designed without drift control, although the ultimate displacement capacity, as shown in Tables 1 and 2, is smaller in the case of drift-controlled buildings. This is because ductility is expressed as the ratio of ultimate displacement to the yield displacement, and the relative reduction in yield displacement is higher as compared to that in the ultimate displacement.

Table 2: Capacity Curve and Capacity Spectrum Parameters for the 9-Storey Buildings

Direction	Design Level	Interstorey Drift at Design Load	Capacity Curve				Capacity Spectrum			
			Yield Point		Ultimate Point		Yield Point		Ultimate Point	
		D_d/H_{tot} (%)	D_y/H_{tot}	V_y/W	D_u/H_{tot}	V_u/W	S_{dy} (mm)	S_{ay} (g)	S_{du} (mm)	S_{au} (g)
Longitudinal	Gravity-Designed	-	0.003	0.012	0.009	0.012	78	0.015	220	0.015
	OMRF, Uncapped Period	0.16	0.004	0.019	0.013	0.018	105	0.023	321	0.022
	OMRF, Capped Period	0.57	0.013	0.064	0.024	0.064	332	0.078	606	0.077
	OMRF, Capped Period (Drift-Controlled)	0.22	0.005	0.079	0.017	0.084	138	0.095	457	0.101
	SMRF, Uncapped Period	0.10	0.004	0.016	0.015	0.013	101	0.019	375	0.016
	SMRF, Capped Period	0.44	0.008	0.040	0.021	0.040	208	0.049	537	0.048
	SMRF, Capped Period (Drift-Controlled)	0.34	0.007	0.041	0.023	0.042	188	0.049	591	0.050
Transverse	Gravity-Designed	-	0.008	0.024	0.014	0.032	193	0.030	352	0.039
	OMRF, Uncapped Period	0.25	0.008	0.032	0.014	0.034	195	0.039	356	0.042
	OMRF, Capped Period	0.64	0.015	0.071	0.021	0.076	374	0.086	535	0.092
	OMRF, Capped Period (Drift-Controlled)	0.34	0.009	0.074	0.018	0.082	232	0.090	461	0.099
	SMRF, Uncapped Period	0.11	0.008	0.024	0.014	0.031	193	0.030	367	0.038
	SMRF, Capped Period	0.54	0.011	0.052	0.020	0.052	286	0.063	510	0.062
	SMRF, Capped Period (Drift-Controlled)	0.40	0.008	0.054	0.020	0.058	195	0.065	511	0.070

Table 3: Ductility and Overstrength Parameters for the 4-Storey Buildings

Design Level	Longitudinal Direction					Transverse Direction				
	Overstrength		Ductility		R_{eff}	Overstrength		Ductility		R_{eff}
	γ	λ	Capacity	Demand		γ	λ	Capacity	Demand	
Gravity-Designed	-	-	3.70	2.44	2.70	-	-	1.74	1.68	1.93
OMRF, Uncapped Period	2.42	2.76	3.99	2.21	2.39	2.93	4.17	1.84	1.65	1.96
OMRF, Capped Period (No Drift Control)	1.96	2.11	2.08	0.80	0.86	1.87	1.98	1.44	0.69	0.79*
OMRF, Capped Period (Drift-Controlled)	2.15	2.36	2.67	0.89	1.06	2.25	2.53	2.09	0.90	1.07
SMRF, Uncapped Period	3.57	4.20	5.27	2.45	2.70	5.73	7.30	1.99	1.45	1.67
SMRF, Capped Period	2.14	2.17	3.52	1.21	1.31	2.14	2.48	2.05	0.97	1.15

*Values of ductility demand and R_{eff} less than unity indicate the elastic response.

Table 4: Ductility and Overstrength Parameters for the 9-Storey Buildings

Design Level	Longitudinal Direction					Transverse Direction				
	Overstrength		Ductility		R_{eff}	Overstrength		Ductility		R_{eff}
	γ	λ	Capacity	Demand		γ	λ	Capacity	Demand	
Gravity-Designed	-	-	2.81	3.53	4.25	-	-	1.83	1.69	2.03
OMRF, Uncapped Period	1.98	1.93	3.05	2.60	2.80	3.57	3.83	1.82	1.65	1.53
OMRF, Capped Period (No Drift Control)	1.60	1.58	1.83	0.75	0.91	1.75	1.88	1.43	0.73	0.76*
OMRF, Capped Period (Drift-Controlled)	1.95	2.07	3.31	1.10	1.24	1.84	2.03	1.99	0.84	1.05
SMRF, Uncapped Period	2.76	2.37	3.71	2.74	3.30	4.51	5.77	1.90	1.48	2.02
SMRF, Capped Period (No Drift Control)	1.67	1.64	2.58	1.18	1.47	2.14	2.13	1.78	0.82*	1.19
SMRF, Capped Period (Drift-Controlled)	1.68	1.72	3.14	1.22	1.57	2.23	2.39	2.62	1.11	1.25

*Values of ductility demand and R_{eff} less than unity indicate the elastic response.

As expected from the equal-displacement principle, the effective reduction factor R_{eff} is almost equal to the ductility demand, which is lower than the ductility capacity by sufficient margins, thus suggesting a satisfactory expected performance by the code-designed buildings. As shown earlier (see Figures 3–8), the expected performance level is that of immediate occupancy for most of the buildings considered in this study and designed as Ordinary Moment-Resisting Frame or Special Moment-Resisting Frame, with period capping and drift control. In some cases, the buildings are expected to remain elastic even during MCE, as indicated by the lower-than-unity ductility demand (see Tables 3 and 4).

The above discussion examines the expected seismic performance of the RC buildings, which have been designed as per the Indian standards, in a deterministic framework. However, this does not provide any idea about the effects of various uncertainties involved in the process of design and construction. The following sections present a discussion on the seismic performance of the RC buildings designed as per the Indian standards in a probabilistic framework.

3. Vulnerability Analysis

Seismic vulnerability (or fragility) of a structure is described as its susceptibility to damage by the ground shaking of a given intensity. It is expressed as a relationship between the ground motion severity (i.e., intensity, PGA, or spectral displacement) and structural damage (expressed in terms of damage grades). Further, it can be expressed as a continuous curve, representing probability distribution for a particular damage grade, or in the form of a damage probability matrix (DPM), representing the discrete probabilities of different damage grades corresponding to a given seismic severity. A number of approaches are available (Calvi et al., 2006) for developing the vulnerability relations for different types of buildings, ranging from those based on the empirical damage data from the past earthquakes to those based on the purely analytical simulations.

The HAZUS methodology, developed for FEMA (NIBS, 1999, 2003) and extensively used the world over in different forms, has been used in the present study to develop vulnerability curves for the RC buildings designed as per the Indian standards. This methodology follows the capacity spectrum formulation, and hence, this can be related with the discussion presented in the previous sections. An important step in developing the fragility curves is the definition of various damage states. On the intensity scales, these damage states are defined in descriptive terms, but for the fragility analysis, these need to be defined in terms of engineering parameters. HAZUS has used a two-criteria approach, which is based on the performance levels of the individual members, for defining the damage state thresholds. Kappos et al. (2006) have proposed a simpler approach (see Table 5) based on the capacity spectrum of the buildings, and the same approach has been used in the present study.

Table 5: Damage-State Definition (Kappos et al., 2006)

Damage Grade	Damage State	Spectral Displacement
DS0	None	$0.7S_{dy} < S_d$
DS1	Slight Damage	$0.7S_{dy} \leq S_d < S_{dy}$
DS2	Moderate Damage	$S_{dy} \leq S_d < 2S_{dy}$
DS3	Substantial-to-Heavy Damage	$2S_{dy} \leq S_d < 0.7S_{du}$
DS4	Very Heavy Damage	$0.7S_{du} \leq S_d < S_{du}$
DS5	Collapse	$S_d > S_{du}$

The vulnerability curves are lognormal distributions representing the probability of attaining or exceeding a given damage state, which is expressed as

$$P\left[ds/S_d\right] = \Phi\left[\frac{1}{\beta_{ds}}\ln\left(\frac{S_d}{\overline{S}_{d,ds}}\right)\right] \tag{4}$$

Here, $\overline{S}_{d,ds}$ is the median spectral displacement for the damage state ds, and Φ is the normal cumulative distribution function. Further, β_{ds} is the standard deviation of the natural logarithm of the spectral displacement for the damage state ds. This describes the combined variability and is expressed as

$$\beta_{ds} = \left\{\left(\mathrm{CONV}\left[\beta_C;\beta_D,\overline{S}_{d,ds}\right]\right)^2 + \left(\beta_{M(ds)}\right)^2\right\}^{1/2} \tag{5}$$

where β_C is the lognormal standard deviation parameter representing variability in the capacity properties of the building, β_D represents the variability in the demand spectrum due to spatial variability of the ground motion, and $\beta_{M(ds)}$ represents the uncertainty in the estimation of damage state threshold.

Each fragility curve is defined by a median value of spectral displacement corresponding to the damage state and the associated variability. The median spectral displacement can be obtained analytically, but the estimation of variability is a complex process requiring statistical data. Naturally, this variability depends on the local conditions and construction practices. HAZUS (NIBS, 2003) has presented variability for the fragility estimation of American (i.e., Californian) buildings. Kappos et al. (2006) have presented a hybrid method for the generation of fragility functions using analytical pushover curves and the earthquake damage data of Greek buildings. Although India has suffered several major earthquakes in the past, unfortunately such systematic data is lacking for the Indian conditions. However, the aim of the present study is not to prescribe the standard fragility functions to be used for the Indian buildings, but to examine the relative role of the different provisions of the Indian seismic code (BIS, 2002). Therefore, the HAZUS values of variability for the relevant cases, as reproduced in Tables 6 and 7, have been considered. In the cases of 'gravity-designed' and Ordinary Moment-Resisting Frame buildings, a major degradation under the seismic loading has been considered, as there is no control on the spacing of stirrups to avoid the low-cycle fatigue rupture of the longitudinal bars under cyclic tension and compression. In the case of the Special Moment-Resisting Frame design, special confining reinforcement is provided in the potential plastic hinge regions, and therefore, variabilities corresponding to the minor post-yield degradation have been considered. Uniform moderate variabilities corresponding to the damage states and capacity curve have been considered in all the cases.

The capacity spectrum parameters presented in Tables 1 and 2 have been used to develop the fragility curves. Figures 9–11 show the fragility curves for different design levels of the 4- and 9-storey buildings. It can be observed that the fragility curves of Ordinary Moment-Resisting Frame and Special Moment-Resisting Frame buildings are crossing each other in some cases, indicating contradictory damage patterns at different ground motion severities. This is a discrepancy arising due to the different variabilities

(Kappos et al., 2006) considered for the two types of design. However, it is also not justifiable to use the same variability for OMRF and SMRF.

Table 6: Variability Parameters Considered for the 4-Storey Buildings (NIBS, 2003)

Design Levels	**Post-yield Degradation (κ)**	**Damage State Variability ($\beta_{M(ds)}$)**	**Capacity Curve Variability (β_c)**	**Total Variability (β_{ds})**
Gravity-Designed	Major Degradation (0.5)	Moderate (0.4)	Moderate (0.3)	0.85
OMRF, Uncapped Period				
OMRF, Capped Period				
OMRF, Capped Period (Drift-Controlled)				
SMRF, Uncapped Period	Minor Degradation (0.9)			0.75
SMRF, Capped Period				
SMRF, Capped Period (Capacity Design)				
SMRF, Equalized Drift				

Table 7: Variability Parameters Considered for the 9-Storey Buildings (NIBS, 2003)

Design Levels	**Post-yield degradation (κ)**	**Damage State Variability ($\beta_{M(ds)}$)**	**Capacity Curve Variability (β_c)**	**Total Variability (β_{ds})**
Gravity-Designed	Major Degradation (0.5)	Moderate (0.4)	Moderate (0.3)	0.80
OMRF, Uncapped Period				
OMRF, Capped Period				
OMRF, Capped Period (Drift-Controlled)				
SMRF, Uncapped Period	Minor Degradation (0.9)			0.70
SMRF, Capped Period				
SMRF, Capped Period (Capacity Design)				
SMRF, Equalized Drift				

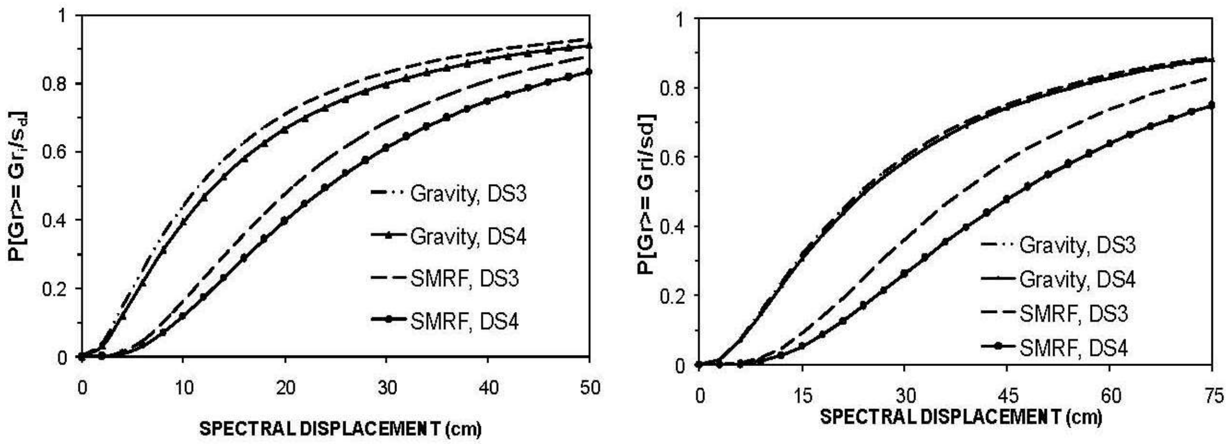

(a) (b)

Fig. 9 Comparison of vulnerability curves for the damage grades DS3 and DS4 and for the buildings designed for gravity load only and as SMRF: (a) 4-storey building; (b) 9-storey building

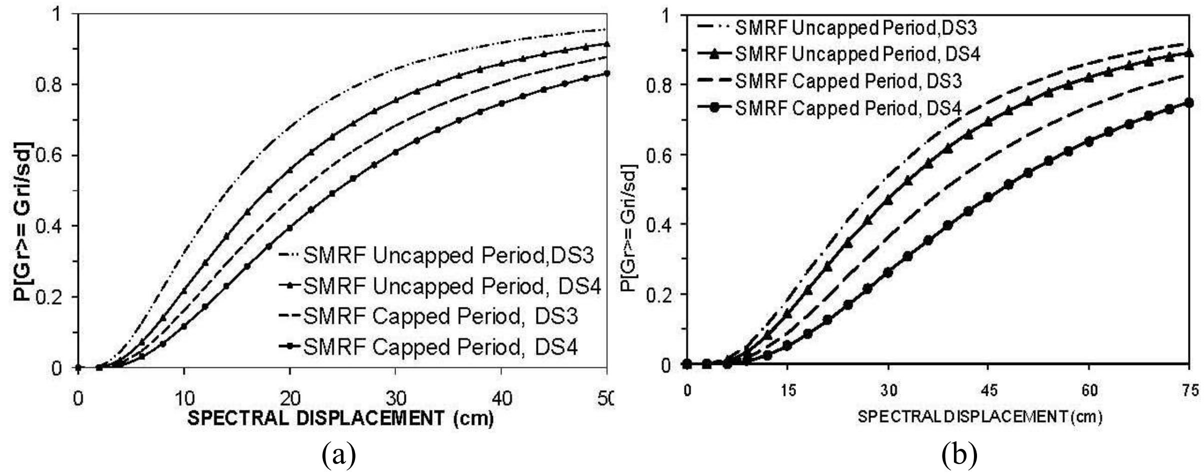

Fig. 10 Effect of period capping on the vulnerability curves for the damage grades DS3 and DS4 and for the SMRF buildings: (a) 4-storey building; (b) 9-storey building

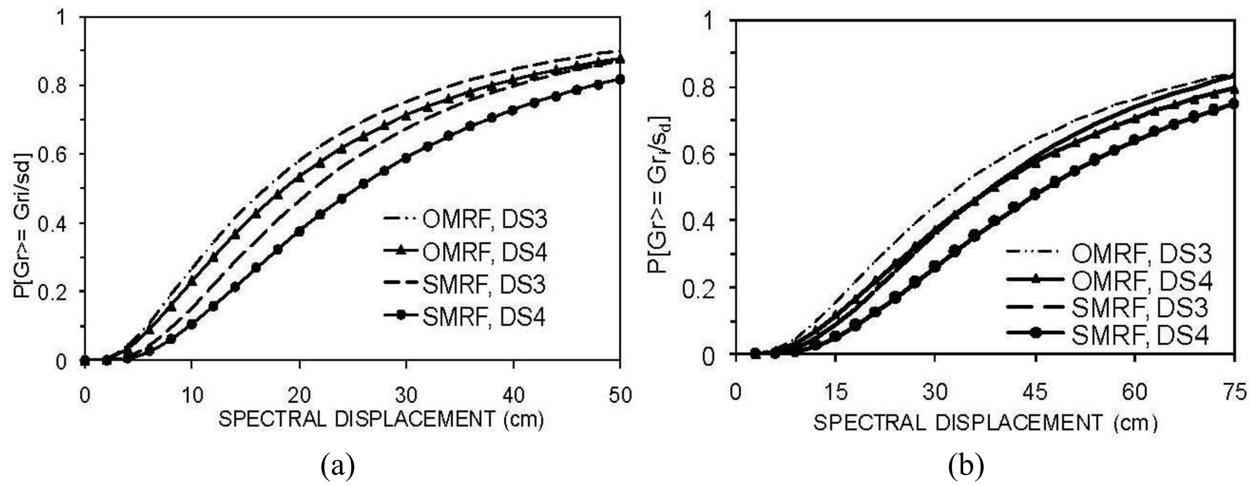

Fig. 11 Comparison of vulnerability curves for the damage grades DS3 and DS4 and for the buildings designed as OMRF and SMRF: (a) 4-storey building; (b) 9-storey building

Tables 8 and 9 show the probabilities of damage being greater than or equal to a particular grade for the 4-storey and 9-storey buildings, respectively, and for the PGA values corresponding to DBE and MCE in different seismic zones. These values have been obtained from the fragility curves, while estimating the spectral displacements corresponding to different PGA values by using the Displacement Modification Method (DMM) of FEMA-440 (FEMA, 2005) and the Indian standard design spectrum (BIS, 2002) at the bedrock. It is interesting to note that the buildings, which have shown the immediate occupancy performance level in the deterministic analysis, have significantly high probability of damage. About 20% buildings designed as per the Indian standards will have some level of damage, even under DBE. Under MCE this damage probability is more than 55%. In case the buildings are subjected to the PGA corresponding to the next higher zone (zone V in this case, with EPGA = 0.36*g*), the damage probability is more than 75%. Further, the damage probability of SMRF buildings is higher than that for the OMRF buildings designed as per the current Indian standards. This is because of higher dependency on ductility, as compared to strength, in the case of SMRF buildings and unequal limits specified in the Indian standard IS 1893 (BIS, 2002) on the total inter-storey drift. The damage probabilities have also been studied by equalizing the total drift in the cases of OMRF and SMRF buildings. It can be observed from Tables 8 and 9 that in this case, there is a significant reduction in the damage probabilities corresponding to the higher grades of damage.

Table 8: Damage Probabilities (%) for the 4-Storey RC Buildings

Design Level	Damage Probability ≥ DS1				Damage Probability ≥ DS3				Damage Probability ≥ DS4			
	PGA (*g*)				PGA (*g*)				PGA (*g*)			
	0.12	**0.18**	**0.24**	**0.36**	**0.12**	**0.18**	**0.24**	**0.36**	**0.12**	**0.18**	**0.24**	**0.36**
Gravity-Designed	52.75	70.75	81.18	91.33	19.94	35.69	48.87	67.32	8.06	30.43	43.11	61.92
OMRF, Uncapped Period	50.10	68.42	79.33	90.23	17.24	32.01	44.86	63.61	5.36	25.45	37.38	56.16
OMRF, Capped Period	18.92	34.31	47.39	65.96	3.70	9.51	16.56	31.05	2.84	7.66	13.79	27.00
SMRF, Uncapped Period	50.18	68.49	79.39	90.27	14.35	27.83	40.15	59.00	2.76	19.05	29.55	47.59
SMRF, Capped Period	23.54	42.83	58.04	77.14	3.44	10.05	18.54	36.16	2.10	6.77	13.37	28.48
SMRF, Equalized Drift	23.98	43.39	58.60	77.57	0.12	0.65	1.79	5.95	0.51	2.12	4.99	13.46

Table 9: Damage Probabilities (%) for the 9-Storey RC Buildings

Design Level	Damage Probability ≥ DS1				Damage Probability ≥ DS3				Damage Probability ≥ DS4			
	PGA (*g*)				PGA (*g*)				PGA (*g*)			
	0.12	**0.18**	**0.24**	**0.36**	**0.12**	**0.18**	**0.24**	**0.36**	**0.12**	**0.18**	**0.24**	**0.36**
Gravity-Designed	53.14	72.09	82.77	92.67	20.74	37.88	52.03	71.15	19.66	36.43	50.50	69.82
OMRF, Uncapped Period	47.83	67.45	79.16	90.64	16.25	31.66	45.32	65.14	14.25	28.70	41.97	61.95
OMRF, Capped Period	14.74	29.43	42.81	62.76	2.11	6.36	12.19	25.50	1.45	4.68	9.39	20.90
SMRF, Uncapped Period	49.18	68.66	80.12	91.19	15.51	30.57	44.10	63.99	11.95	25.12	37.78	57.75
SMRF, Capped Period	19.88	39.48	55.73	76.53	1.91	6.76	13.95	30.73	0.93	3.79	8.62	19.62
SMRF, Equalized Drift	26.62	48.20	64.27	82.77	0.08	0.52	1.58	5.83	0.37	1.81	4.61	13.26

CONCLUSIONS

This paper has examined the effects of various provisions of the Indian standards on the seismic performance of RC buildings in deterministic and probabilistic terms. The widely known shortcoming of the Indian standard IS 13920 (BIS, 1993) of having inadequate capacity design provisions regarding the strong column-weak beam design has not been considered in this study as it is already well-researched. The fragility functions presented in this study are not intended to be used as the standard functions for loss estimation, as those need to be first calibrated with the statistical data for the Indian conditions.

The RC buildings designed as per the Indian standards have the overstrength ratio of the order of 2, which results in a significant reserve strength. It has been shown that the buildings, which are properly designed and constructed as per the Indian standards for the gravity loads only, can generally survive a seismic excitation up to MCE of the zone IV without collapse.

The buildings designed as OMRF or as SMRF, as per the Indian standards, satisfy the immediate occupancy performance level, even for Maximum Considered Earthquake. Interestingly, the performance of OMRF design is marginally better than that of the SMRF design. The current provision for limiting the interstorey drift at the design loads is responsible for this discrepancy. Capping on the design period, as specified by the code (BIS, 2002), is the most crucial provision for controlling the expected performance of the buildings. This results in more than two-times increase in the design base shear.

The deterministic framework does not provide adequate insight into the expected performance of the buildings. The buildings showing the immediate occupancy performance levels in the deterministic analysis have shown significantly high damage probabilities on considering the inherent variabilities in the capacity and demand.

The current form of the Indian standard provisions for the control of interstorey drift leads to many discrepancies. This governs the design, only when capping on the design period is applied, although the buildings designed with period-capping are generally stiffer than the buildings designed without capping. Further, this is generally not a governing criterion in the case of SMRF, in spite of the fact that the SMRF design results in more flexible buildings. In probabilistic terms, this results in a higher probability of damage in the case of SMRF design as compared to the OMRF design. This discrepancy is due to the specification of interstorey drift limit at the design loads, which results in different effective limits on the inelastic drifts in the cases of OMRF and SMRF.

In probabilistic terms also, the performance of OMRF design is marginally better than that of the SMRF design. However, the performance of SMRF design is improved significantly, particularly at the higher ground shaking levels, by controlling the inelastic drift. Therefore, the current provision of Indian standard IS 1893 (BIS, 2002) regarding the limit on interstorey drift needs revision.

REFERENCES

1. ACI (2008). “Building Code Requirements for Structural Concrete (ACI 318M-08) and Commentary”, ACI Standard, American Concrete Institute, Farmington Hills, U.S.A.
2. ASCE (2006). “ASCE/SEI 7-05: Minimum Design Loads for Buildings and Other Structures”, ASCE Standard, American Society of Civil Engineers, Reston, U.S.A.
3. ASCE (2007). “ASCE/SEI 41-06: Seismic Rehabilitation of Existing Buildings”, ASCE Standard, American Society of Civil Engineers, Reston, U.S.A.
4. BIS (1987a). “IS: 875 (Part 1)-1987—Indian Standard Code of Practice for Design Loads (Other than Earthquake) for Buildings and Structures, Part 1: Dead Loads—Unit Weights of Building Materials and Stored Materials (Second Revision)”, Bureau of Indian Standards, New Delhi.
5. BIS (1987b). “IS: 875 (Part 2)-1987—Indian Standard Code of Practice for Design Loads (Other than Earthquake) for Buildings and Structures, Part 2: Imposed Loads (Second Revision)”, Bureau of Indian Standards, New Delhi.
6. BIS (1993). “IS 13920: 1993—Indian Standard Ductile Detailing of Reinforced Concrete Structures Subjected to Seismic Forces—Code of Practice”, Bureau of Indian Standards, New Delhi.
7. BIS (2000). “IS 456: 2000—Indian Standard Plain and Reinforced Concrete—Code of Practice (Fourth Revision)”, Bureau of Indian Standards, New Delhi.
8. BIS (2002). “IS 1893 (Part 1): 2002—Indian Standard Criteria for Earthquake Resistant Design of Structures, Part 1: General Provisions and Buildings (Fifth Revision)”, Bureau of Indian Standards, New Delhi.
9. BSI (2004). “BS EN 1998-1:2004—Eurocode 8: Design of Structures for Earthquake Resistance, Part 1: General Rules, Seismic Actions and Rules for Buildings”, British Standards Institution, London, U.K.
10. Calvi, G.M., Pinho, R., Magenes, G., Bommer, J.J., Restrepo-Vélez, L.F. and Crowley, H. (2006). “Development of Seismic Vulnerability Assessment Methodologies over the Past 30 Years”, ISET Journal of Earthquake Technology, Vol. 43, No. 3, pp. 75–104.
11. Chopra, A.K. and Goel, R.K. (2002). “A Modal Pushover Analysis Procedure for Estimating Seismic Demands for Buildings”, Earthquake Engineering & Structural Dynamics, Vol. 31, No. 3, pp. 561–582.
12. CSI (2006). “SAP2000: Integrated Software for Structural Analysis & Design, Version 10.0.5—Analysis Reference Manual”, Computers and Structures, Inc., Berkeley, U.S.A.
13. FEMA (2000). “Prestandard and Commentary for the Seismic Rehabilitation of Buildings”, Report FEMA 356, Federal Emergency Management Agency, Washington, DC, U.S.A.

14. FEMA (2005). “Improvement of Nonlinear Static Seismic Analysis Procedures”, Report FEMA 440, Federal Emergency Management Agency, Washington, DC, U.S.A.
15. ICC (2006). “International Building Code”, International Code Council, Washington, DC, U.S.A.
16. Kappos, A.J., Panagopoulos, G., Panagiotopoulos, C. and Penelis, G. (2006). “A Hybrid Method for the Vulnerability Assessment of R/C and URM Buildings”, Bulletin of Earthquake Engineering, Vol. 4, No. 4, pp. 391–413.
17. NIBS (1999). “Earthquake Loss Estimation Methodology HAZUS: Technical Manual”, Report Prepared for the Federal Emergency Management Agency, National Institute of Building Sciences, Washington, DC, U.S.A.
18. NIBS (2003). “Multi-hazard Loss Estimation Methodology, Earthquake Model—HAZUS-MH: Technical Manual”, Report Prepared for the Federal Emergency Management Agency, National Institute of Building Sciences, Washington, DC, U.S.A.
19. Park, R. and Paulay, T. (1975). “Reinforced Concrete Structures”, John Wiley & Sons, Inc., New York, U.S.A.
20. Priestley, M.J.N. (1993). “Myths and Fallacies in Earthquake Engineering—Conflicts between Design and Reality”, Bulletin of the New Zealand Society for Earthquake Engineering, Vol. 26, No. 3, pp. 329–341.
21. Priestley, M.J.N. (2000). “Performance Based Seismic Design”, Proceedings of the 12th World Conference on Earthquake Engineering, Auckland, New Zealand, Paper No. 2831 (on CD).
22. Priestley, M.J.N. (2003). “Myths and Fallacies in Earthquake Engineering, Revisited: The Mallet Milne Lecture, 2003”, IUSS Press, Pavia, Italy.
23. Priestley, M.J.N., Calvi, G.M. and Kowalsky, M.J. (2007). “Displacement-Based Seismic Design of Structures”, IUSS Press, Pavia, Italy.
24. Qi, X. and Moehle, J.P. (1991). “Displacement Design Approach for Reinforced Concrete Structures Subjected to Earthquakes”, Report UCB/EERC-91/02, University of California, Berkeley, U.S.A.